Chapter 12

Mechanical Coating Technique for Composite Films and Composite Photocatalyst Films

Yun Lu, Liang Hao and Hiroyuki Yoshida

Additional information is available at the end of the chapter

http://dx.doi.org/10.5772/48794

1. Introduction

1.1. Coating techniques for film materials and their applications

In the field of materials science and engineering, the investigation on film materials is becoming increasingly important. By film materials, we can develop a variety of new material properties in the fields of electrics and electronics, optics, thermotics, magnetic, and mechanics, among others (S. Yoshida et al., 2008). In recent years, without the development of film materials we could not make any great progress in the renewable energy, environment improvement, exploitation of space, and so on. The coating techniques for film materials can fall into several categories as shown in Table 1.

In these techniques, physical vapor deposition (PVD) and chemical vapor deposition (CVD) are most widely applied. PVD are atomistic deposition processes in which material is vaporized from a solid or liquid source in the form of atoms or molecules and transported in the form of a vapor through a vacuum or low pressure gaseous (or plasma) environment to the substrate, where it condenses. PVD can be used to deposit films of elements and alloys as well as compounds using reactive deposition processes (Mattox, 2010). On the other hand, CVD may be defined as the deposition of a solid on a heated surface from a chemical reaction in the vapor phase. It belongs to the class of vapor-transfer processes which is atomistic in nature, which is the deposition species are atoms or molecules or a combined of these (Pierson, 1999). Microfabrication processes widely use CVD to deposit film materials in various forms including monocrystalline, polycrystalline, amorphous and epitaxial depending on the deposition materials and the reaction conditions. As listed in Table 1, there are other coating techniques for film materials such as liquid absorption coating, thermal spraying and mechanical coating. However, their applications are narrow comparing with PVD and CVD due to their features.

Physical vapor deposition (PVD)	Vacuum deposition	Resistance heating, Flash Evaporation, Vacuum Arc, Laser heating, Highfrequency heating, Electron beam heating
	MBE（Molecular Beam Epitaxy）	
	Laser deposition	
	Sputter deposition	Ion beam sputtering, DC sputtering, Highfrequency sputtering, Magnetron sputtering, Microwave ECR plasma deposition
	Ion beam plating	Highfrequency ion plating, Activated reactive evaporation, Arc ion plating
	Ion beam deposition	
	Ionized cluster beam deposition	
Chemical vapor deposition (CVD)	Thermal CVD	Atmospheric pressure CVD, Low pressure CVD
	Plasma CVD	DC plasma CVD, Highfrequency plasma CVD, Microwave plasma CVD, ERC plasma CVD
	Photo-excited CVD	
Liquid absorption coating	Plating	Electroplating, Electroless plating
	Anodic oxide coating, Painting, Sol-gel method	
	Spin coating, Dip coating, Roll coating, Spry coating	
Thermal spraying	Flame spraying, Electrical spraying (Arc, Plasma)	
Mechanical coating	Shot coating, Powder impact plating, Aerosol deposition , Gas deposition	

Table 1. Classification of the coating techniques for film materials

1.2. Advantages and limitations of these coating techniques

Any film coating technique has its advantages and limitations. The features of these coating techniques make their application fields different. Their advantages and limitations are summarized and shown in Table 2. Thickness control and coating of large-area films can be achieved in PVD which has become the major film coating technique in the fields of electronics, electrics and optics industries due to its high production efficiency, high film purity and low production cost. However, complicated and large scale equipments are necessary. In addition, films cannot be deposit on the substrates with complex profiles. In CVD processes, films can deposit on the substrates with complex profiles and the adhesion between films and substrates is generally strong. However, the processes are performed at temperature of 600 ºC and above. Large scale equipments are also needed just as PVD processes. The advantages and limitations of other coating techniques can also be found in Table 2. We will not explain them in detail any more.

Film coating technique	Advantages	Limitations
PVD	Thickness control Large area coating	Large and complex equipment Coating on flat substrate
CVD	Coating on complex substrate Strong adhesion	Large and complex equipment Elevated temperature process
Liquid absorption coating	Simple equipment Coating on complex substrate	Complicated post treatment Elevated temperature process
Thermal spraying	Rapid coating Large specific area	Elevated temperature process Grain growth
Mechanical coating	Ambient preparation Nanoscale coating	Large and complex equipment Coating on flat substrate

Table 2. Advantages and limitations of the film coating techniques

2. A novel coating technique for composite films

2.1. Proposal of a novel coating technique

2.1.1. Contamination phenomena during Mechanical Alloying (MA)

Powder metallurgy has been widely used in the manufacturing of mechanical parts. A typical process of powder metallurgy is shown in Fig. 1. As shown in the schematic diagram, blending of powder particles is necessary before compacting. Ball milling is often used to mix powder particles and make them homogeneous. Mechanical alloying, well known as ball milling, is frequently used to improve various material properties and to prepare advanced materials that are different or impossible to be obtained by traditional techniques (Suryanarayana, 2001). Ceramic balls are often used as grinding mediums which are indispensable in MA. However, the contamination of powder from grinding mediums and the adhesion of powder particles to the grinding mediums always harass engineers. Especially, the adhesion of powder particles to the grinding mediums and the bowl is really difficult to be eliminated.

2.1.2. Concept proposal of mechanical coating technique (MCT)

From the contamination discussed above, we proposed a novel film coating technique in 2005 called mechanical coating technique (MCT) with the diagram schematic shown in Fig. 2 (Lu et al., 2005). In this technique, metal powder and ceramic grinding mediums (balls, buttons and columns) are used as the coating material and the substrates respectively. Firstly, they are charged into a bowl made of alumina. The mechanical coating is performed by a pot mill or a planetary ball mill. In the process, friction, wear and impact among metal powder particles, ceramic grinding mediums and the inner wall of the bowl occur. That results in the formation of metal films on ceramic grinding mediums. In fact, some other

researchers prepared metal or alloy films on grinding mediums by this technique. Kobayashi prepared metallic films on ZrO_2 balls (Kobayashi, 1995). Romankov et al. (2006) deposited Al and Ti-Al coatings on Ti alloy substrates. Gupta et al. (2009) reported the formation of nanocrystalline Fe-Si coatings on mild steel substrates. Farahbakhsh et al. (2011) prepared Cu and Ni-Cu solid solution coatings on Ni balls. Mechanical coating technique performed by ball milling has been established and known. After the proposal of MCT in 2005, we have made some important progress in advancing it. Titanium films on ceramic balls have been fabricated and their properties have been investigated (Yoshida et al., 2009 a). By MCT and its following high-temperature oxidation, TiO_2/Ti composite photocatalyst films have been successfully prepared (H. Yoshida et al., 2008). After that, we proposed 2-step MCT to fabricate TiO_2/Ti composite photocatalyst films without high-temperature oxidation (Lu et al., 2011). In addition, 2-step MCT was also used to fabricate TiO_2/Cu composite photocatalyst films (Lu et al., 2012). In this chapter, we will give a brief introduction to MCT, 2-step MCT and the relevant processes as a novel technique to fabricate composite films and TiO_2/metal composite photocatalyst films.

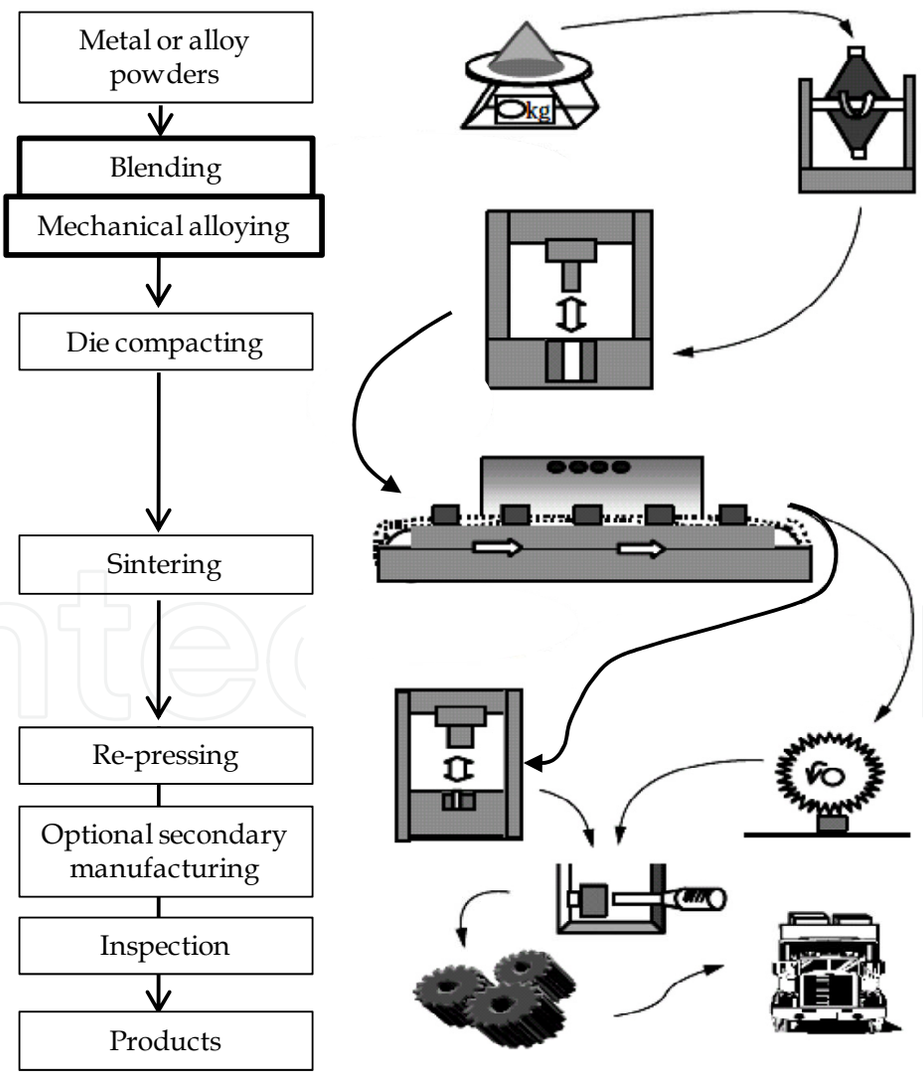

Figure 1. Simplified flowchart and schematic diagram of a typical powder metallurgy process

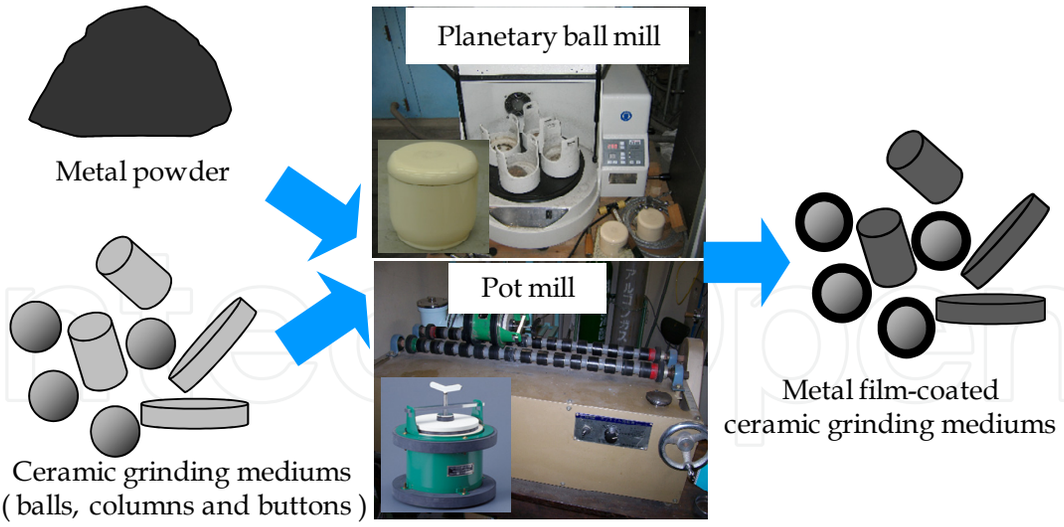

Figure 2. Schematic diagram of mechanical coating technique (MCT)

2.2. MCT and its influencing parameters

In our early work, we fabricated Ti films on alumina (Al_2O_3) grinding mediums such as balls, buttons and columns. Ti powder and Al_2O_3 grinding mediums were used as the coating materials and the substrates respectively. They were charged into a bowl made of alumina with the dimension of Φ75 × 90 mm (400 *ml*). The mechanical coating was carried out by a pot mill with a rotation speed of 80 rpm for 1000 h. Fig. 3 (a) shows the appearance comparison of the Al_2O_3 grinding mediums before and after MCT. It can be clearly seen that the Al_2O_3 grinding mediums after MCT showed metallic luster which means metal films might be formed on these grinding mediums. Also, the appearances of metal-coated Al_2O_3 balls after high-temperature oxidation are given in Fig. 3 (b).

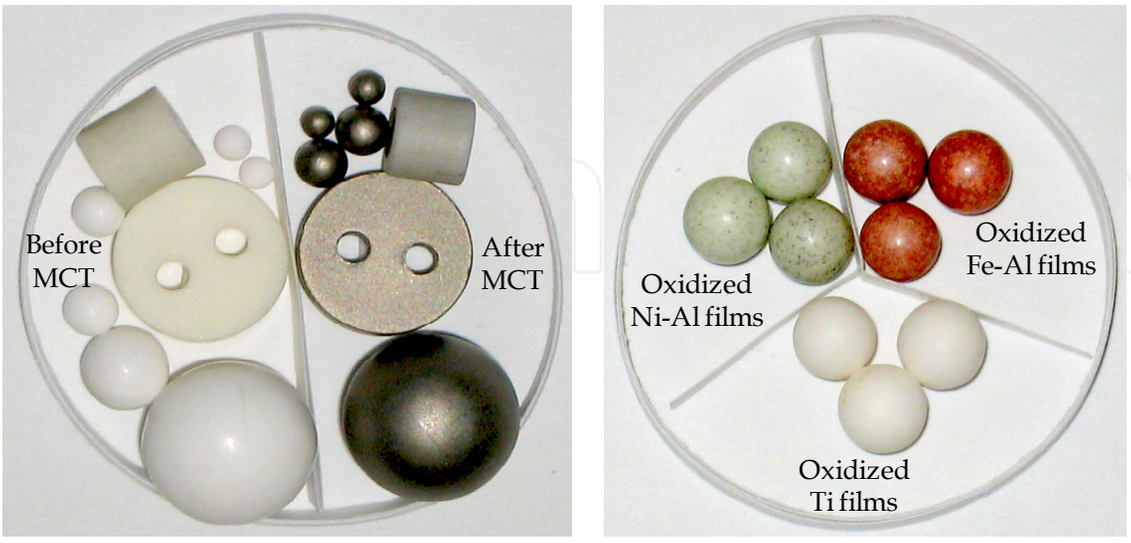

(a) Alumina objects before and after MCT

(b) Alumina balls after MCT and the following high-temperature oxidation

Figure 3. Appearances of Al_2O_3 grinding mediums after MCT and high-temperature oxidation

The influencing parameters of MCT include:

1. Impact force or impact energy: type of mill, milling speed, milling container, milling time, grinding medium, extent of filling the bowl, ball-to-powder weight ratio
2. Physic, chemical and mechanical properties of powder and grinding mediums
3. Milling atmosphere and milling temperature

2.3. Characterization of Ti films fabricated by MCT

2.3.1. Appearance, microstructure and thickness of the Ti films

Fig. 4 shows the appearances of the Al_2O_3 balls after MCT. It can be seen that the color of the Al_2O_3 balls changed from white to metallic gray as MCT time increased. It means that more Ti powder particles adhered to the surfaces of the Al_2O_3 balls. Impact force of only about 1 G can be obtained during MCT performed by pot mill. When it is carried out by planetary ball mill, impact force over 10 G or even 40 G can be realized. Therefore, the required time to form metal films can be decreased greatly in the case of planetary ball mill. The SEM images of the cross sections of the Ti-coated Al_2O_3 balls are also given in Fig. 5. With the increase of MCT time, the film thickness increased. The surface morphologies of the Ti film-coated

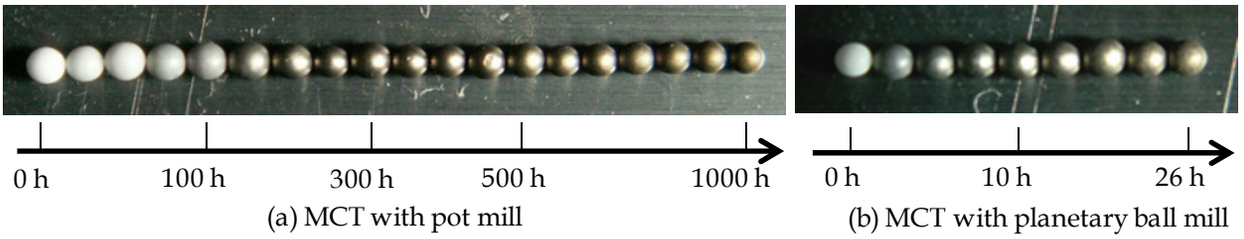

Figure 4. Appearances of the Ti-coated Al_2O_3 balls during MCT for different MCT time

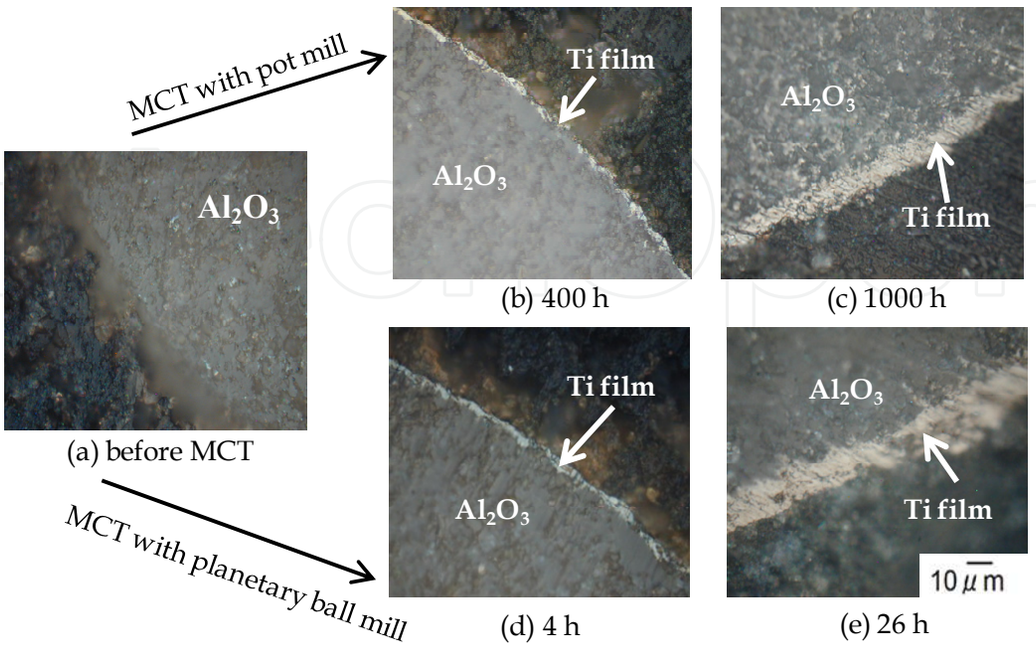

Figure 5. SEM images of the cross sections of the Ti film-coated Al_2O_3 balls during MCT

Al_2O_3 balls are shown in Fig. 6. Discrete Ti particles adhered to the surfaces of Al_2O_3 balls and they connected with each other. The irregular surface can result in high specific area. The thickness evolution of Ti films during MCT was also monitored and is illustrated in Fig. 7. No matter in the case of pot mill or planetary ball mill, the film thickness increased with the increase of MCT time. They reached 10 and 12 μm respectively in pot mill and planetary ball mill after 1000 h and 26 h. Therefore, it is possible to control the film thickness by MCT.

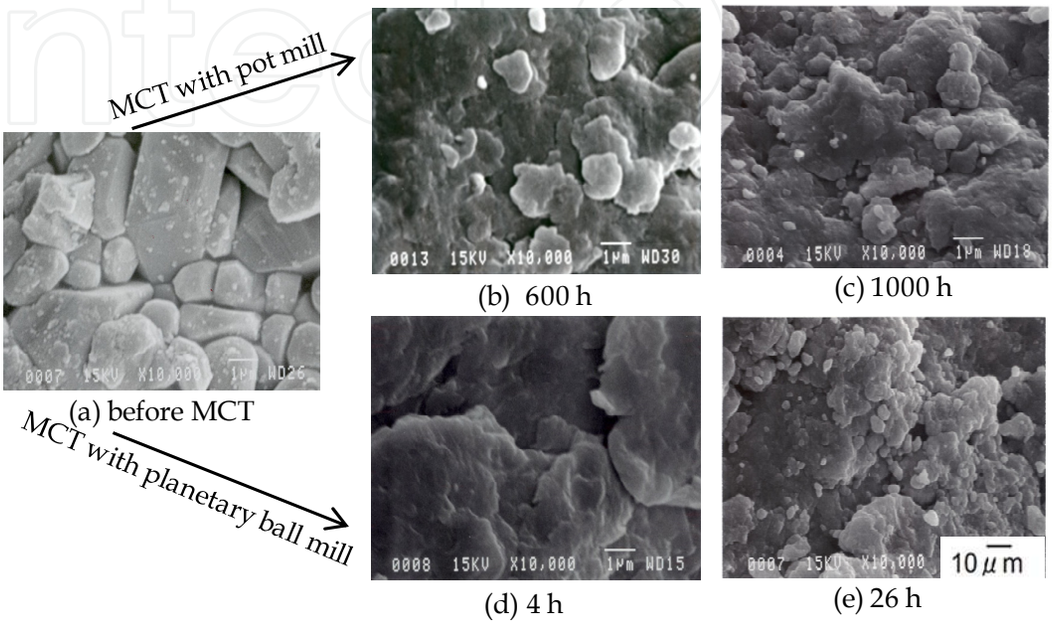

Figure 6. Surface morphologies of Ti film-coated Al_2O_3 balls during MCT

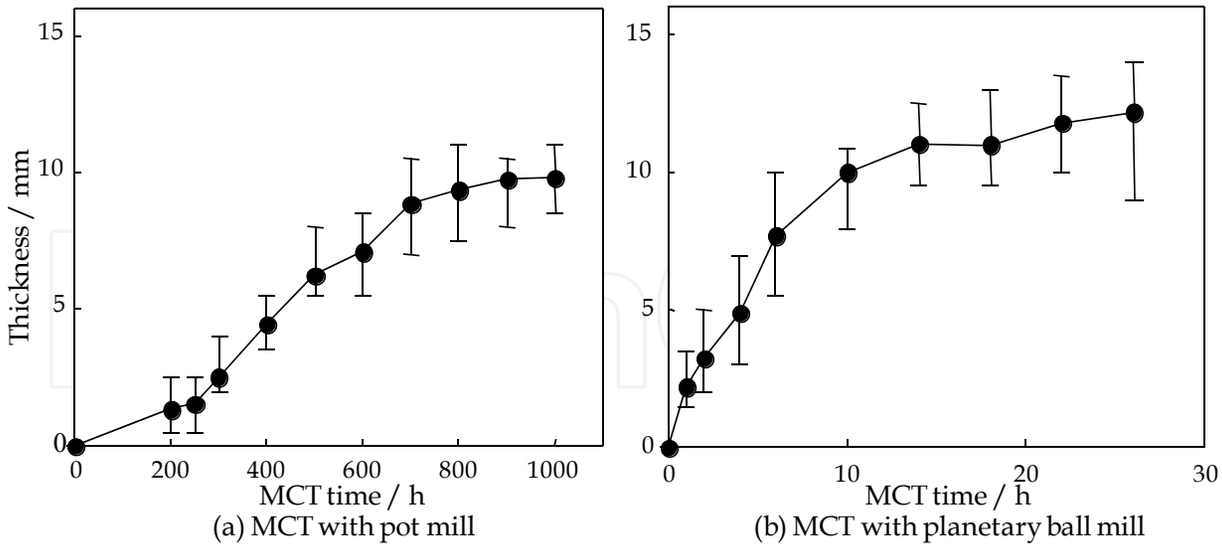

Figure 7. Thickness evolution of Ti films as a function of MCT time

2.3.2. Electrical resistance of the Ti films

Electrical resistance is one important property of film materials. Four-point probe method is frequently used to measure electrical resistance of films on a flat substrate (JIS K 7194, 1994).

However, this method is only applicable to planar films. It cannot used to measure the electrical resistance of spherical films. Therefore, we proposed a new electrical resistance determination method of spherical films such as Ti films on Al_2O_3 balls. By this method, we established the relationship between electrical resistivity and film thickness.

The determination method is shown in Fig. 8. Two plate probes contacts the Ti film-coated Al_2O_3 ball (Φ 1 mm) along the direction of tangential line. To decrease contact resistance, a pressure force of 800 gf is loaded along the normal direction of the ball. The press force is determined in pre-experiments. Electrical resistance is measured for 10 times by changing the contact points between the two plate probes and the ball. In addition, the measurement on electrical resistance is carried out for three randomly chosen Ti film-coated Al_2O_3 balls. The average value of the measurements for 30 times is used as the electrical resistance of the Ti film. Fig. 9 shows the evolution of electrical resistance of the Ti film-coated Al_2O_3 balls during MCT by pot mill and planetary ball mill. For the both cases, the electrical resistance decreased with the increase of MCT time.

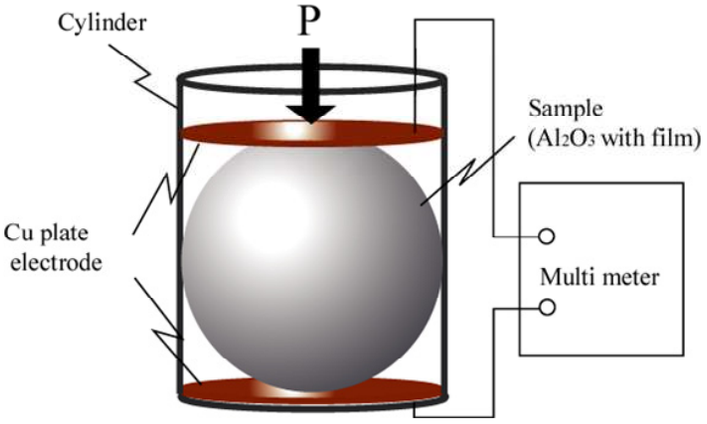

Figure 8. Measurement of electrical resistance of the Ti film-coated Al_2O_3 balls

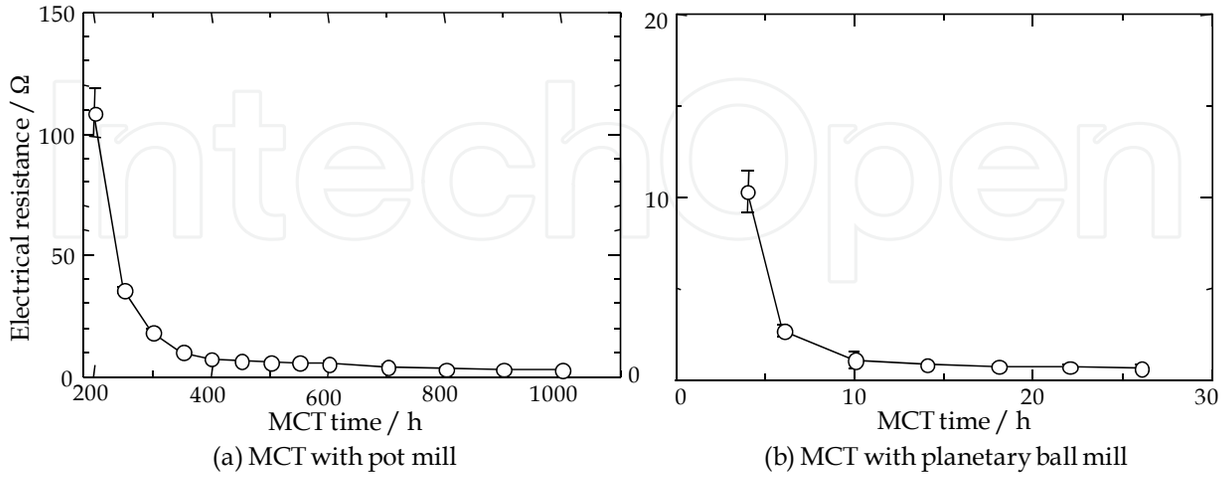

Figure 9. Electrical resistance of the Ti film-coated Al_2O_3 balls

To establish the relationship between electrical resistance and film thickness, we proposed a spherical shell model for Ti film-coated Al_2O_3 ball as shown in Fig. 10. Here *r* is the radius of

Al_2O_3 ball, h is the film thickness. Therefore, the electrical resistance of the spherical Ti films on Al_2O_3 ball $z = +(r+h)$ to $z = -(r+h)$ can be given by

$$R = \int_{-(r+h)}^{+(r+h)} \rho \frac{dz}{A} = 2\int_{0}^{+(r+h)} \left(\rho \frac{dz}{A_1} + \rho \frac{dz}{A_2}\right) \tag{1}$$

Where ρ is the electrical resistivity of the films, A_1 is the ring area of the films in the range of $0 \le z \le r$, and A_2 is the area of the circle crossed with vertical axis z in the range of $r < z \le r+h$. Electrical resistance in the range of $0 \le z \le r$ and $r < z \le r+h$ can be defined as R_1 and R_2 respectively and can be given by

$$R_1 = \int_0^r \rho \frac{dz}{A_1} = \int_0^r \frac{\rho}{\pi} \frac{dz}{(r+h)^2 - r^2} \tag{2}$$

$$R_2 = \int_r^{r+h} \rho \frac{dz}{A_2} = \int_r^{r+h} \frac{\rho}{\pi} \frac{dz}{(r+h)^2 - z^2} \tag{3}$$

During the measurement of electrical resistance shown in Fig. 8, the contact of the plate probes and Al_2O_3 ball should not be a point but a plane which has a certain area. It is proper to give the integral calculus from r to C ($r < C \le r+h$).

$$R_2 = \int_r^C \frac{\rho}{\pi} \frac{dz}{(r+h)^2 - C^2} = \frac{\rho}{2\pi(r+h)} \ln \left| \frac{(r+h)^2 - C^2}{(r+h)^2 - r^2} \right| \tag{4}$$

The electrical resistance of the spherical Ti films on an Al_2O_3 ball can be given by

$$R = 2(R_1 + R_2) = 2\left\{ \frac{\rho}{\pi} \frac{r}{(r+h)^2 - r^2} + \frac{\rho}{2\pi(r+h)} \ln \left| \frac{(r+h)^2 - C^2}{(r+h)^2 - r^2} \right| \right\} \tag{5}$$

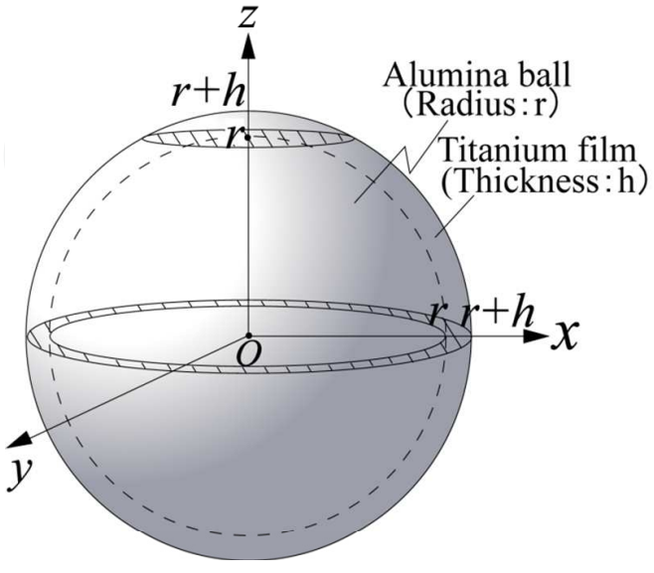

Figure 10. Spherical shell model for the electrical resistance of the Ti film-coated Al_2O_3 balls

Therefore, we can calculate electrical resistivity, ρ of the film by Eq. 5 using the measured electrical resistance of the films, R and the film thickness, h. Fig. 11 shows the relationship between the electrical resistivity of the Ti films and their thickness. It can be found that the electrical resistivity went down and then kept a constant. The evolution of the electrical resistivity should result from the density evolution of the films. In the case of planetary ball mill, the stable electrical resistivity was smaller than that in the case of pot mill. That should be due to the higher film density obtained in the circumstance of larger impact force in the case of planetary ball mill.

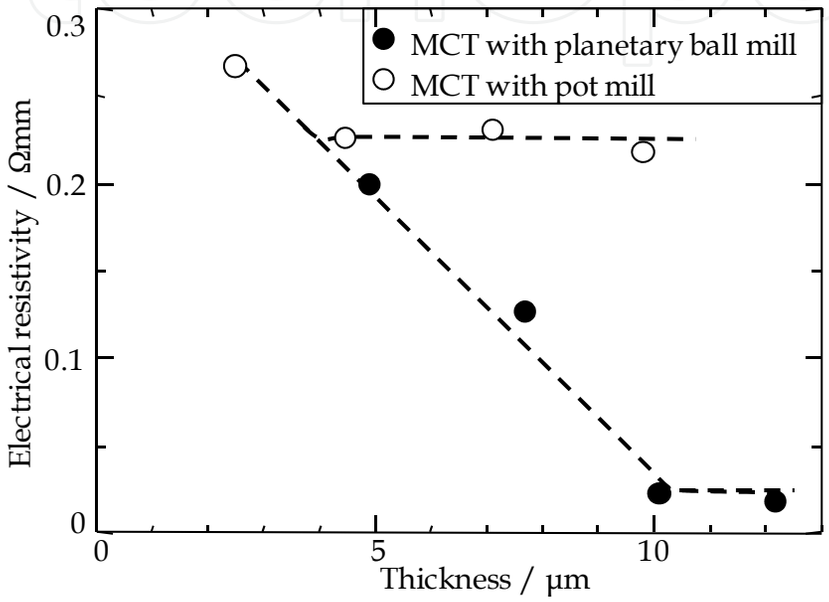

Figure 11. Relationship between electrical resistivity of Ti films and their thicknesses

2.4. TiO_2/Ti composite films fabricated by MCT and the following high-temperature oxidation

We successfully fabricated TiO_2/Ti composite films by MCT and the following high-temperature oxidation. Firstly, Ti films were prepared by MCT shown in Fig. 2. Subsequently, the Ti film-coated Al_2O_3 balls were oxidized at high temperatures. In this section, we will introduce the fabricate processes and the characterization of the TiO_2/Ti composite films.

2.4.1. Fabrication processes

Ti powder with a purity of 99.9% and an average diameter of 30 μm was used as the coating material. Al_2O_3 balls with an average diameter of 1 mm were used as the substrates. A planetary ball mill (P5/4, Fritsch) was used to perform MCT (Yoshida, 2009 b). 40 g Ti powder and 60 g Al_2O_3 balls were charged into a bowl made of alumina with a dimension of Φ75×70 mm (250 *ml*). MCT was carried out with a rotation speed of 300 rpm for 10 h. The obtained Ti film-coated Al_2O_3 balls were denoted as M10-Ti. To form TiO_2 films, the M10-Ti

samples were oxidized in air at 573, 623, 673, 723, 773, 873 and 973 K for 20 h. Here the samples were denoted as M10-*T*-20. *T* means the oxidation temperature. The samples after MCT and the following high-temperature oxidation were examined by SEM (JEOL, JSM-6100) and XRD (JEOL, JDX-3530). Cu-*Kα* radiation in the condition of 30 kV and 30 mA was used for XRD. Before the characterization, all the samples were cleaned in acetone by ultrasonic (frequency: 28 kHz) to remove Ti and TiO_2 that did not adhere strongly.

2.4.2. Characterization of the TiO_2/Ti composite films

Fig. 12 shows the appearances of the M10-Ti and M10-*T*-20 samples. The color of the M10-*T*-20 samples changed with increase of oxidation temperature and lost metallic luster comparing with M10-Ti. The color change indicates that the degree of oxidation was different at different oxidation temperature. The M10-573-20 samples showed brown color which was similar to that of TiO. That means the oxidation of Ti films at 573 K was insufficient. When oxidation temperature was increased to 673, 723, 773 and 873 K, the samples color changed from blue to gray. It was probably related to the growth of TiO_2 crystalline and the film thickness increase. Besides, the color of M10-973-20 samples was light yellow. It indicates that titanium was completely oxidized to titanium dioxide.

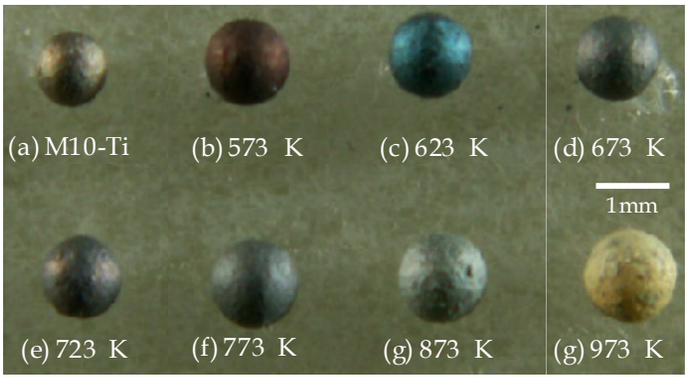

Figure 12. Appearances of M10-Ti and M10-*T*-20 samples

The surface SEM images of the samples are shown in Fig. 13. From Fig. 13(a), the Ti films had uneven surfaces comparing with those prepared by PVD or CVD. The surface evolution with the increase of oxidation temperature can be seen from Fig. 13(b) to (f). It seems that the surface crystals grew up with the increase of oxidation temperature. However, column nanocrystals were formed at 973 K. Fig. 14 shows the XRD patterns of the samples after MCT and the following high-temperature oxidation. The diffraction intensity of Ti peaks decreased with the increase of oxidation temperature and the Ti peak at about 41° (2θ) disappeared when oxidation temperature was increased to 973 K. Conversely, the peaks of rutile TiO_2 appeared when oxidation temperature was above 673 K and the diffraction intensity became stronger as oxidation temperature increased. From the above results, it can be concluded that the films had a composite microstructure of Ti and rutile TiO_2 when oxidation temperature was between 673 and 873 K. TiO_2/Ti composite films on Al_2O_3 balls were fabricated by MCT and the following high-temperature oxidation.

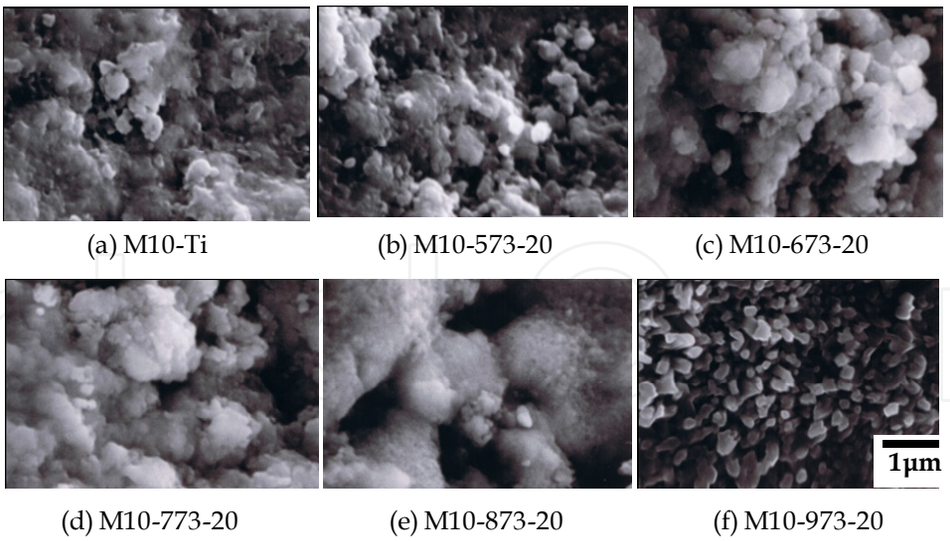

Figure 13. Surface SEM images of M10-Ti and M10-*T*-20 samples

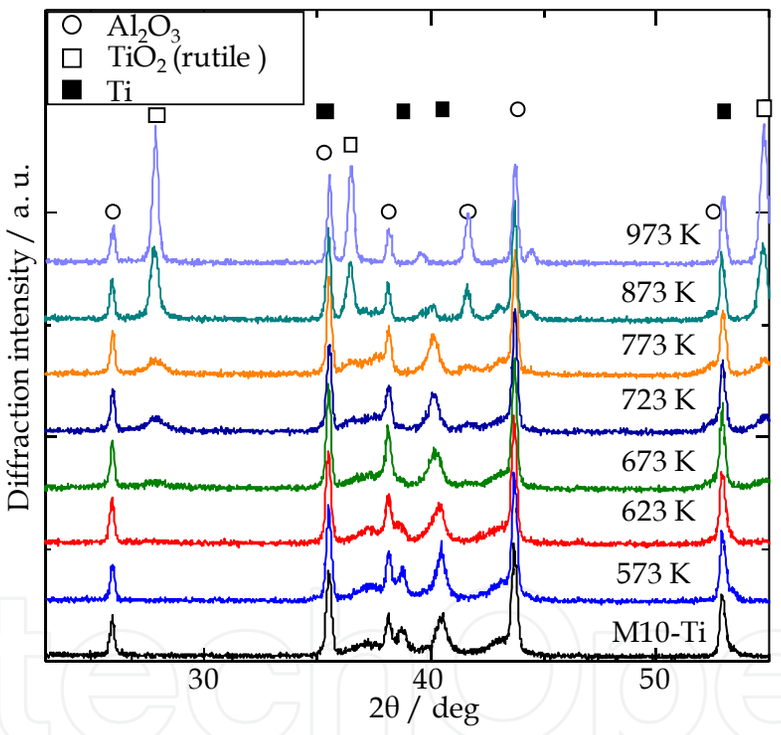

Figure 14. XRD patterns of M10-Ti and M10-T-20 samples

2.5. 2-step Mechanical Coating Technique (2-step MCT)

An advanced mechanical coating technique called 2-step mechanical coating technique (2-step MCT) was developed to fabricate TiO_2/Ti composite films. As anatase TiO_2 cannot be easily obtained by oxidation, we aim to deposit anatase TiO_2 on Ti films directly by MCT. In this section, we will introduce the processes of 2-step MCT and characterize the composite films. The influences of 2nd step MCT time and the introduction of ceramic impact balls on the composite films and their photocatalytic activity were also discussed.

2.5.1. Processes of 2-step MCT

The schematic diagram of 2-step MCT is shown in Fig. 15. In the first step, Ti films are prepared on the surfaces of Al_2O_3 balls as our previous work (Lu et al., 2005 & Yoshida et al., 2009 a). The source materials and their relevant parameters are listed in Table 3. 40 g Ti powder and 60 g Al_2O_3 balls are used as the coating material and the substrates respectively. A planetary ball mill (P5/4, Fritsch) is used to perform MCT. The experimental condition has been discussed in Section 2.4.1. In the second step, TiO_2/Ti composite films are fabricated. 15 g Ti film-coated Al_2O_3 balls and 13 g TiO_2 powder are used as the substrates and the coating material respectively. The relevant parameters can be found in Table 3. They are charged into a bowl made of alumina. Then the coating of TiO_2 is performed by the same planetary ball mill with a rotation speed of 300 rpm for 1, 3, 6 and 10 h. To investigate the influence of average diameter of TiO_2 powder on the photocatalytic activity of the composite films, two kinds of anatase TiO_2 powder with different average diameter are used as the coating materials. To understand the influence of impact force on the formation and the photocatalytic activity of TiO_2/Ti composite films, Al_2O_3 or WC impact balls with the diameter of 10 mm are also introduced into the second step of 2-step MCT. The relevant denotations are listed in Table 4.

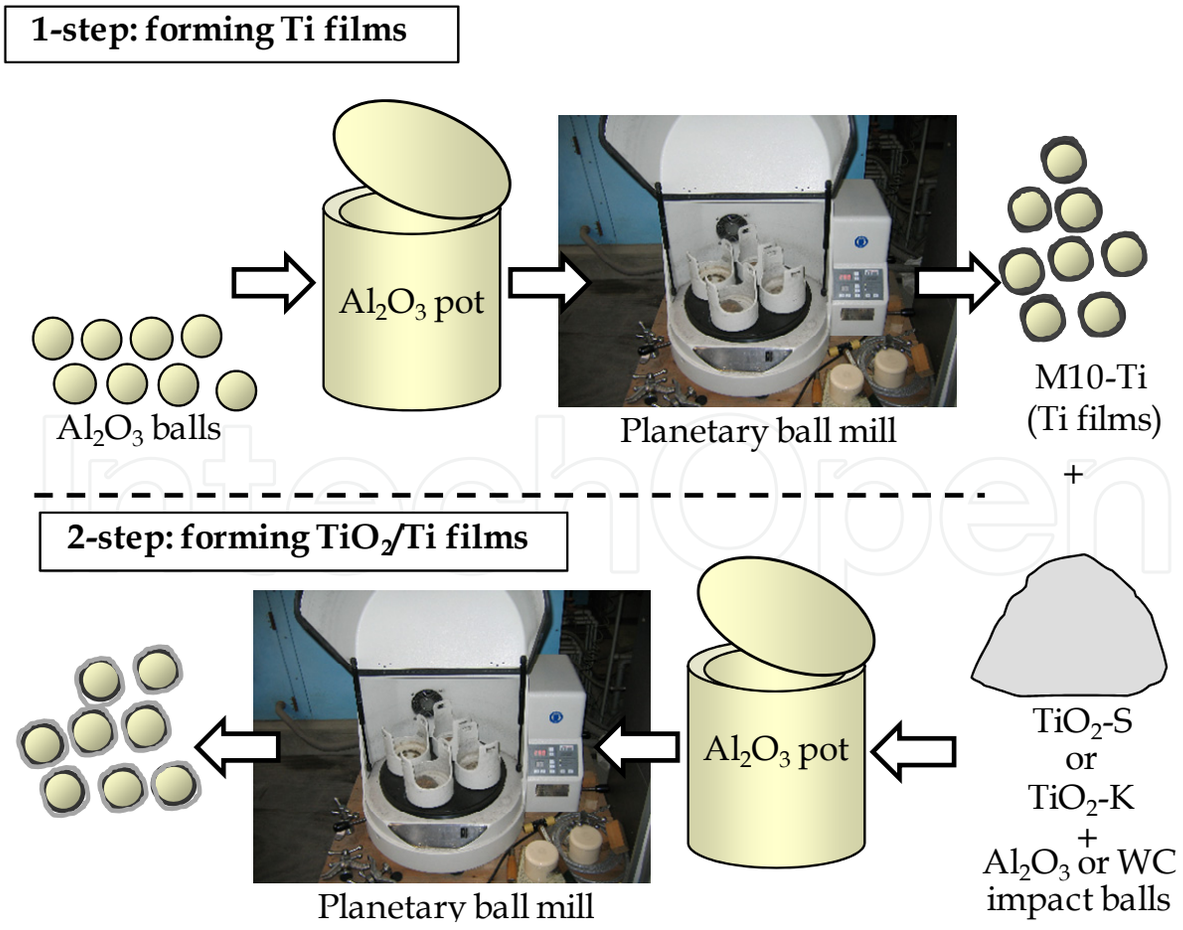

Figure 15. Schematic diagram of 2-step MCT for the fabrication of TiO_2/Ti composite films

Ti powder	Purity: 99.1% Average diameter: 30 μm
Substrate	ϕ1 Al_2O_3 balls Purity: 93.0%
TiO_2 powder (anatase)	Average diameter: 7 nm (TiO_2-S)
	Average diameter: 0.45 μm (TiO_2-K)

Table 3. Source materials for the fabrication of TiO_2/Ti composite films by 2-step MCT

TiO_2 powder	Impact ball	Sample denotation
TiO_2-S		CM*x*S
	Al_2O_3	ϕ10A-CM*x*S
	WC	ϕ10W-CM*x*S
TiO_2-K		CM*x*K
	Al_2O_3	ϕ10A-CM*x*K
	WC	ϕ10W-CM*x*K

Note: *x* is the 2nd step MCT time.

Table 4. Sample denotations for the fabrication of TiO_2/Ti composite films by 2-step MCT

2.5.2. TiO_2/Ti composite films fabricated by 2-step MCT without impact balls

Fig. 16 shows the appearances of the Al_2O_3 balls after 2-step MCT without ceramic impact balls. The color of the samples changed and lost metallic luster with the increase of the 2nd step MCT time. The CM3S samples showed different colors from place to place on the surface. However, the CM6S and CM10S samples showed uniform color respectively. It hints that uniform composite films might form at that time. Fig. 17 shows the surface SEM images of the samples fabricated by 2-step MCT without ceramic impact balls. From Fig. 17(a), the gray areas correspond to Ti. It can be seen that uniform Ti films have been formed on the surface of Al_2O_3 ball. From Fig. 17(b) and (c), the white and gray areas correspond to Ti and TiO_2 respectively. Continuous TiO_2 films were not form while TiO_2 deposited on Ti films in the form of discrete island. Meanwhile, the SEM images of the cross sections of the samples fabricated by 2-step MCT without ceramic impact balls are shown in Fig. 18. It can be clearly seen that Al_2O_3 balls were coated with Ti films and discrete islands of TiO_2 adhered to the Ti films. A composite microstructure of Ti and TiO_2 was formed. During the impact between Al_2O_3 balls or Al_2O_3 ball and the inner wall of the bowl, TiO_2 powder particles were trapped between them. Under the great impact force, TiO_2 particles were inlaid into the Ti films. It results in the formation of the TiO_2/Ti composite microstructure. Fig. 19 shows the XRD patterns of the samples after 2-step MCT without impact balls. When the 2nd step MCT time was 1 h, the peaks of anatase TiO_2 appeared which means that TiO_2 particles had adhered to Ti films. As it came to 3 h, the intensity of anatase TiO_2 peaks

reached their highest values. It indicates that the loading amounts of TiO_2 in the TiO_2/Ti composite films reached the maximum values. After that, the TiO_2 peaks became lower which should be due to the exfoliation of TiO_2 that coated Ti films. From the above results, the films had a composite microstructure of Ti and TiO_2. The loading amounts of TiO_2 in the composite films changed with the increase of the 2nd step MCT time. 2-step MCT is a simple and applicable technique to fabricate TiO_2/Ti composite films.

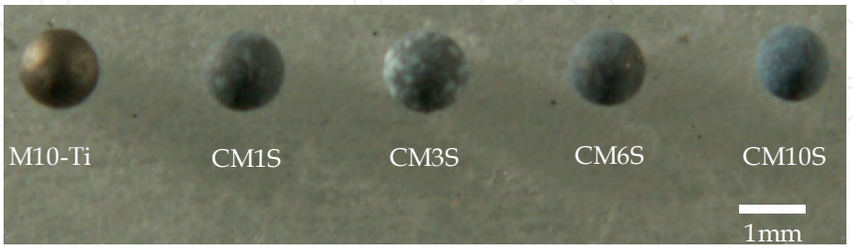

Figure 16. Appearances of the samples after 2-step MCT

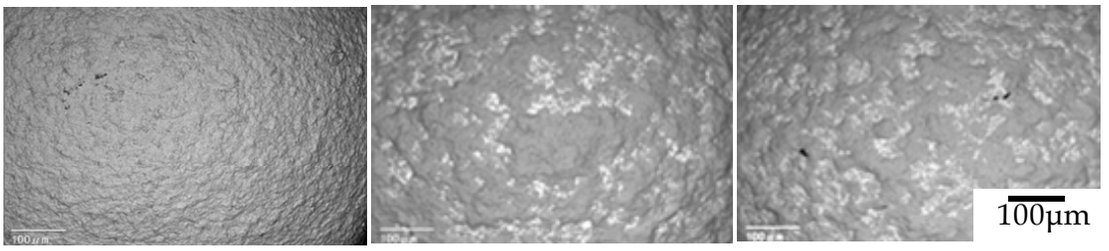

(a) M10-Ti (b) CM3S (c) CM10S

Figure 17. SEM images of the surfaces of the samples fabricated by 2-step MCT

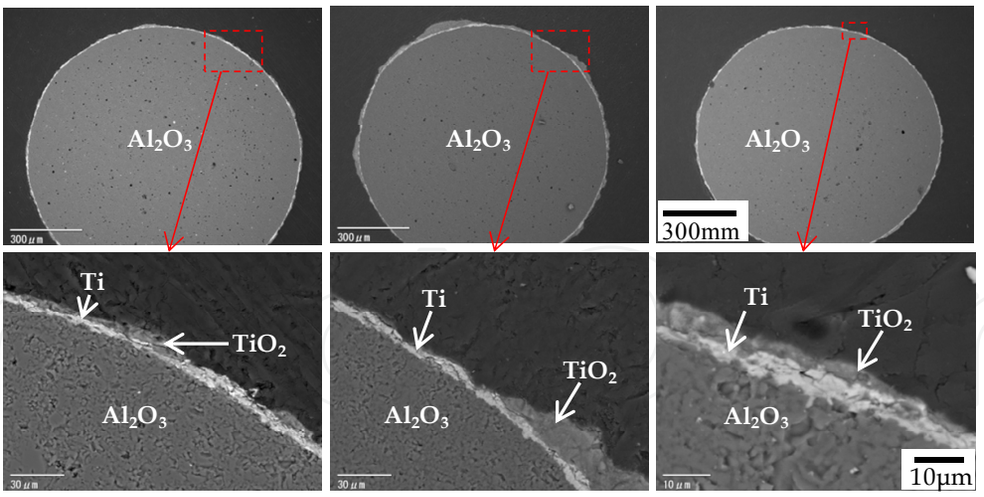

(a) CM1S (b) CM3S (c) CM6S

Figure 18. SEM images of the cross sections of the samples fabricated by 2-step MCT

2.5.3. TiO_2/Ti composite films fabricated by 2-step MCT with impact balls

Fig. 20 shows the appearances of the Al_2O_3 balls after 2-step MCT with ceramic impact balls. The samples lost metallic luster and their colors changed. That hints TiO_2/Ti composite films might be formed. Fig. 21 shows the SEM image of the cross section of the TiO_2/Ti composite

films fabricated by 2-step MCT with WC impact balls. It can be seen that the films had a composite microstructure of Ti film and discrete islands of TiO_2. The surface condition of the composite films fabricated with TiO_2 powder with different average diameters are compared in Fig. 22. The distribution of TiO_2 powder particles with the average diameter of 0.45 μm were more uneven under the impact of WC balls compared with those with the average diameter of 7 nm. Φ10W-CM6K sample had a high hardness of 472 (dynamic hardness) on the cross section. It was close to that of alumina. It hints that the composite films were very hard.

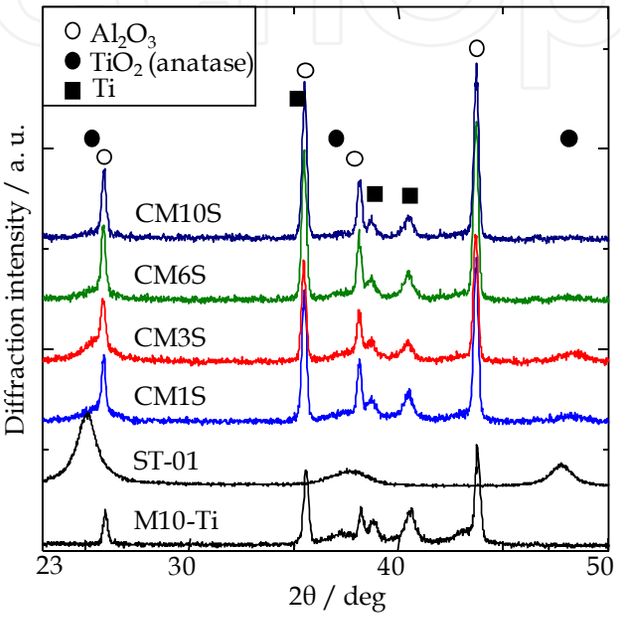

Figure 19. XRD patterns of the samples fabricated by 2-step MCT

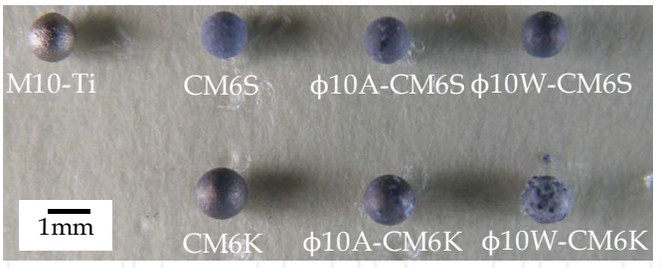

Figure 20. Appearances of the samples fabricated by 2-step MCT

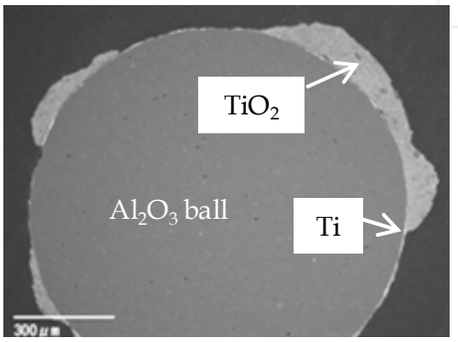

Figure 21. SEM image of the cross section of the Φ10W-CM6K sample fabricated by 2-step MCT

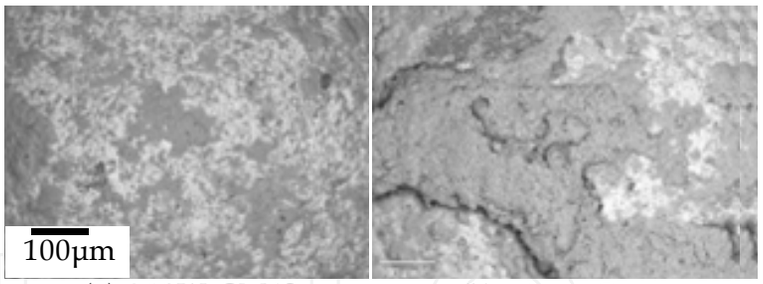

(a) ϕ10W-CM6S (b) ϕ10W-CM6K

Figure 22. Surface SEM images of the samples fabricated by 2-step MCT

The XRD patterns of the samples fabricated with TiO_2 powder of different average diameters by 2-step MCT with WC impact balls are given in Fig. 23. In the case of nano-sized TiO_2 powder (Fig.23 (a)), the peaks of Ti and TiO_2 can be found. On the other hand, the diffraction peaks of TiO_2 cannot be detected for the micron-sized TiO_2 powder (Fig.23 (b)). It means the loading amounts of TiO_2 in the composite films were rather small.

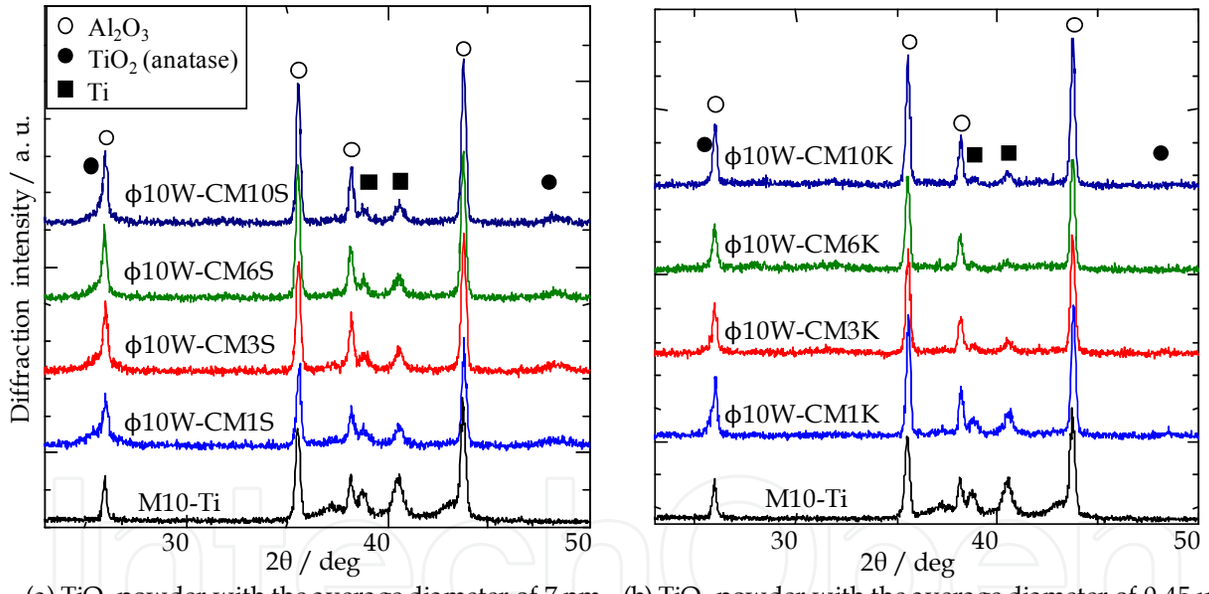

(a) TiO_2 powder with the average diameter of 7 nm (b) TiO_2 powder with the average diameter of 0.45 μm

Figure 23. XRD patterns of the samples fabricated by 2-step MCT with WC impact balls

3. Photocatalytic activity of TiO_2/metal composite films

Although the photocatalytic activity of TiO_2 under ultraviolet and visible light irradiation has been investigated around the world, only the photocatalytic activity of TiO_2/metal composite films under ultraviolet irradiation is involved and discussed in this section. Here, we developed evaluation method of photocatalytic activity of TiO_2/metal composite films by which we evaluated the photocatalytic activity of TiO_2/Ti and TiO_2/Cu composite films fabricated by MCT.

3.1. Evaluation method of photocatalytic activity

We developed evaluation method of photocatalytic activity of the TiO_2/metal composite films by referring to Japan Industrial Standard (JIS R 1703-2, 2007). The evaluation procedure is as follows. Before the evaluation of photocatalytic activity, pre-adsorption of methylene blue (MB) is carried out to obtain the same initial evaluation condition for all the samples. Firstly, the cleaned samples are dispersed uniformly to form a layer of samples on the bottom of a cylinder-shaped cell with a dimension of Φ18 × 50 mm. Subsequently, 3 *ml* MB solution with a concentration of 20 *μmol/l* is poured into the cell. The cell with the samples and MB solution is kept in a totally dark place for 12 h. Then, the evaluation of the photocatalytic activity will be carried out. The samples after pre-adsorption are laid uniformly on the bottom of a same cell to form a layer of samples and 7 *ml* MB solution with a concentration of 10 *μmol/l* is poured into the cell. The schematic diagram of the evaluation of photocatalytic activity is shown in Fig. 24. A colorimeter (Sanshin Industrial Co., Ltd) of 660 nm in UV radiation wavelength, which is near the peak of absorption spectrum of MB solution (664 nm), is used to measure the absorbance of MB solution. The UV irradiation time is 24 h. Besides, both of the pre-adsorption and the evaluation of photocatalytic activity are carried out at room temperature. The gradient, *k* of MB solution concentration-irradiation time curve is calculated by the least-squares method with the data from 1 to 12 h and *k* is used as the degradation rate constants. The higher the degradation rate constants *k*, the higher the photocatalytic activity.

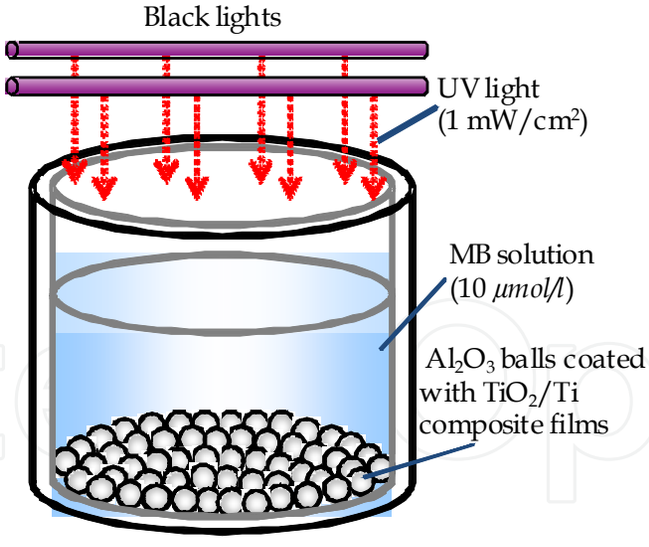

Figure 24. Photocatalytic activity evaluation of TiO_2/metal composite films fabricated by MCT

3.2. Photocatalytic activity of TiO_2/Ti composite films

Fig. 25 shows the evolution of MB solution concentration as UV irradiation time under the action of TiO_2/Ti composite films fabricated by MCT and its following high-temperature oxidation as described in Section 2.4. MB solution concentration slight increased in the case of M10-Ti and M10-573-20. Meanwhile, MB solution concentration decreased in varying

degrees in the case of the other samples. That means MB was degraded under the action of UV light and TiO_2 samples. In other word, the samples fabricated by MCT and its following high-temperature oxidation showed photocatalytic activity.

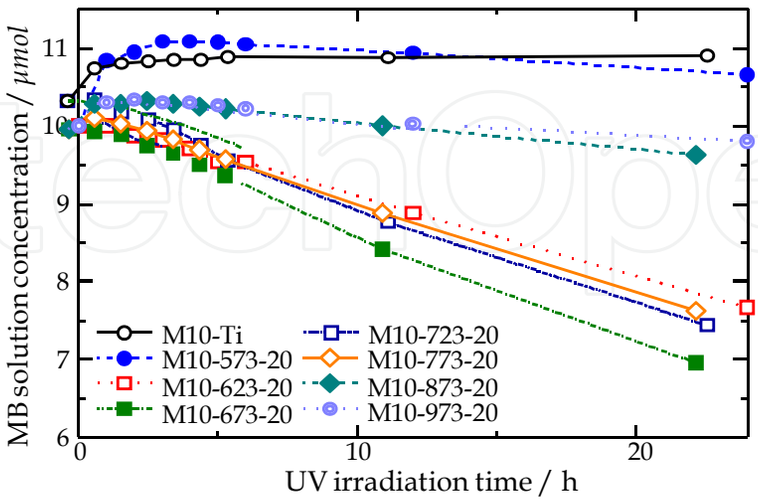

Figure 25. MB solution concentration as a function of UV irradiation time under the action of the samples fabricated by MCT and the following high-temperature oxidation

The degradation rate constants, k are also given in Fig. 26. It can be seen that the degradation rate constants, k increased with the increase of oxidation temperature and reached the peak value at 723 K above which the degradation rate constants, k decreased. Combined with the XRD patterns in Fig. 14, the evolution of the photocatalytic activity can be discussed as follows. When oxidation temperature was below 623 K, the peaks of TiO_2 were not detected which means Ti films were not oxidized or were oxidized sufficiently. Therefore, the photocatalytic activity of the films was low as shown in Fig. 26. With the increase of oxidation temperature from 623 to 773 K, more Ti films were oxidized and TiO_2/Ti composite films were formed. The improvement of photocatalytic activity should relate to the composite microstructure of TiO_2 and Ti. According to charge separation effect (Rengaraj et al., 2007), electrons in TiO_2 may transfer to metals with higher work functions. The electron transfer can decrease the recombination velocity of electron-hole pairs in TiO_2. It can improve the photocatalytic activity of TiO_2. When oxidation temperature was 723 K, the composite films obtained the optimum ratio of TiO_2 to Ti. It resulted in the highest photocatalytic activity. When oxidation temperature was above 773 K, the oxidation degree of Ti films was further increased and Ti films were completely oxidized when oxidation temperature was above a certain value. Although the amounts of TiO_2 increased, the photocatalytic activity decreased due to the weakening of charge separation effect.

The degradation rate constants, k as a function of 2nd step MCT time are shown in Fig. 27. In the case of nano-sized TiO_2 powder (Fig. 27(a)), the samples fabricated without ceramic impact balls showed the highest photocatalytic activity and the degradation rate constants, k exceeded 350 nmol·l^{-1}·h^{-1}. After the introduction of ceramic impact balls into 2-step MCT, the photocatalytic activity was decreased. On the other hand, the samples fabricated with Al_2O_3 impact balls showed the greatest photocatalytic activity in the case of micron-sized TiO_2

powder (Fig. 27(b)). Compared with the TiO_2/Ti composite films fabricated with micron-sized TiO_2 powder, the composite films fabricated with nano-sized TiO_2 powder showed much higher photocatalytic activity. It should relate to the higher specific area of nano-sized TiO_2 powder particles. From Fig. 26 and 27, anatase TiO_2/Ti composite films showed much higher photocatalytic activity than that of rutile TiO_2/Ti composite films. It is well known that anatase TiO_2 generally shows higher photocatalytic activity than rutile TiO_2.

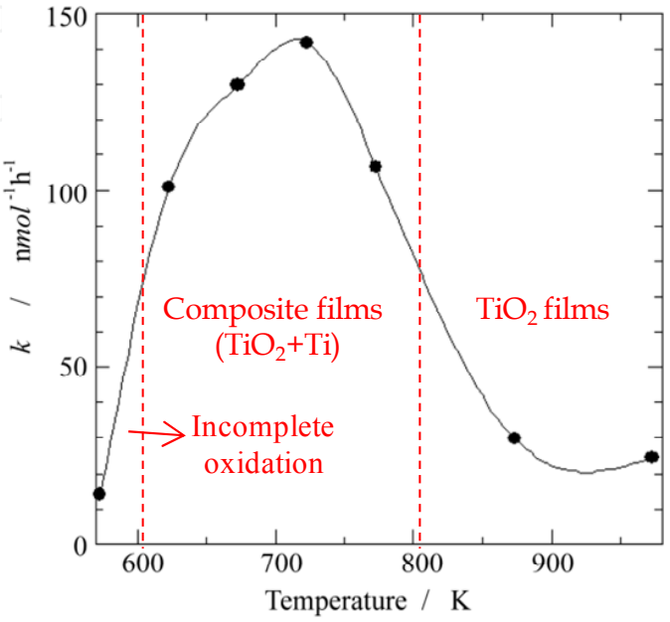

Figure 26. Degradation rate constants, *k* as a function of oxidation temperature

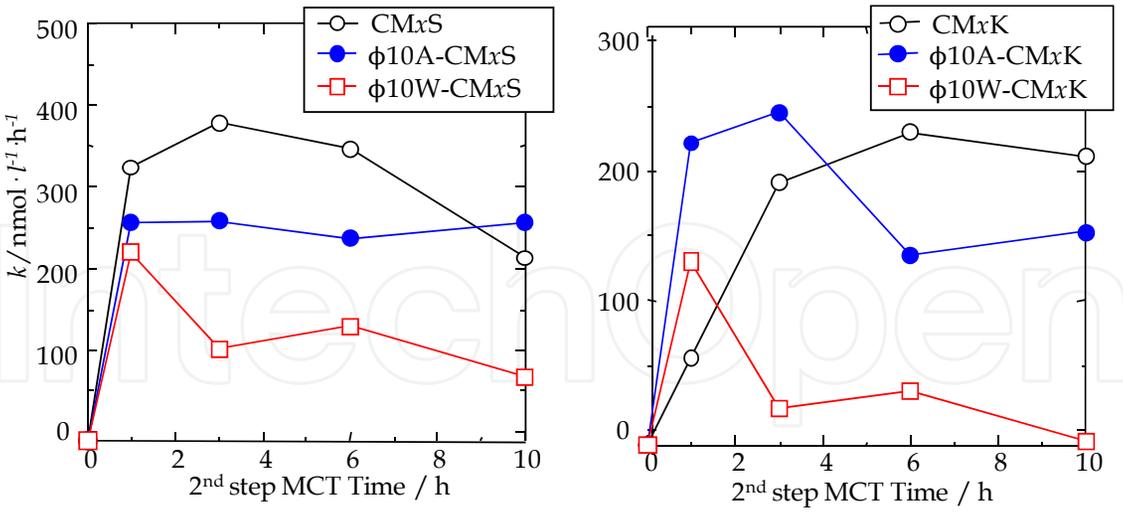

(a) TiO_2 powder with the average diameter of 7 nm (b) TiO_2 powder with the average diameter of 0.45 μm

Figure 27. Degradation rate constants, *k* as a function of 2nd step MCT time

3.3. Improvement of photocatalytic activity by high-temperature oxidation

High-temperature oxidation was carried out to increase the crystallinity and the volumes of TiO_2 in TiO_2/Ti composite films fabricated by 2-step MCT and therefore improve the

photocatalytic activity of the composite films (Lu et al., 2011 b). The composite films after the high-temperature oxidation were characterized and their photocatalytic activity was also evaluated. In addition, the effect on high-temperature oxidation on the microstructure and the photocatalytic activity of the composite films was also discussed.

3.3.1. Improved fabrication processes

Firstly, TiO_2/Ti composite films were prepared by 2-step MCT as described in Section 2.5.1. Ti powder with a purity of 99.1% and an average diameter of 30 μm was used as the coating material. Al_2O_3 balls with an average diameter of 1 mm were used as the substrates. After the formation of Ti films on Al_2O_3 balls, anatase TiO_2 powder with an average diameter of 0.45 μm (Kishida Chemical Co. Ltd., Japan) was used to form TiO_2/Ti composite films. To make the composite films strong enough, Al_2O_3 or WC balls with the diameter of 10 mm were introduced into the fabrication of the composite films. The schematic diagram can be seen in Fig. 15. Subsequently, high-temperature oxidation was carried out for the TiO_2/Ti composite films fabricated by 2-step MCT. The oxidation temperature was set at 673, 773 and 873 K and the oxidation time was 10 h. The denotations of the samples fabricated by 2-step MCT and the following high-temperature oxidation are listed in Table 5.

TiO_2 powder	Impact ball	Sample maker
TiO_2-K	---	CM*x*K-*y*
	Al_2O_3	ϕ10A-CM*x*K-*y*
	WC	ϕ10W-CM*x*K-*y*

Note: *x* means the 2nd step MCT time, *y* is oxidation temperature.

Table 5. Denotations of the samples fabricated by 2-step MCT and the following high-temperature oxidation

3.3.2. Characterization of the TiO_2/Ti composite films

Fig. 28 shows the appearances of the samples fabricated by 2-step MCT and the following high-temperature oxidation. The samples lost metallic luster and became white compared with the Ti film-coated Al_2O_3 balls. Also, dark and uneven areas can also be seen. The surface SEM images of the samples are shown in Fig. 29. The surface color of the samples seems to be uniform except for some point areas. It indicates that the uniform TiO_2 films were formed. However, for the TiO_2/Ti composite films fabricated by 2-step MCT there are light and dark areas corresponding to Ti and TiO_2 respectively shown in Fig. 17.

The SEM images of the cross sections of the samples are given in Fig. 30. It can be seen that a composite microstructure of TiO_2 films and Ti films formed. In other words, TiO_2/Ti composite films were fabricated. The TiO_2 films consisted of the deposited TiO_2 in the second step of 2-step MCT and the TiO_2 formed in high-temperature oxidation. From the above results, it can be concluded that the loading amounts of TiO_2 in the composite films were increased by high-temperature oxidation.

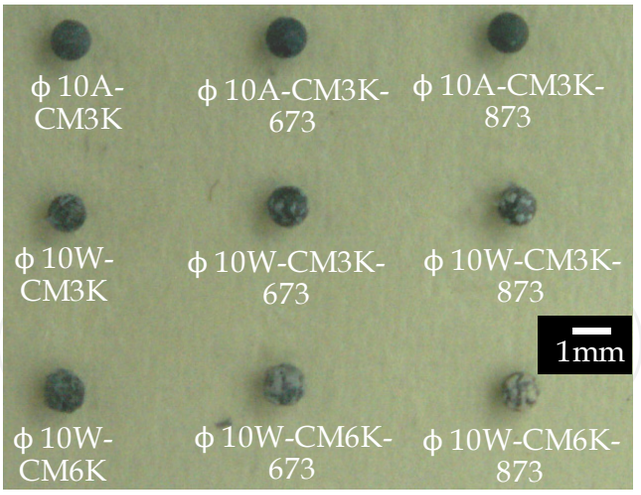

Figure 28. Appearances of the samples fabricated by 2-step MCT and the following high-temperature oxidation

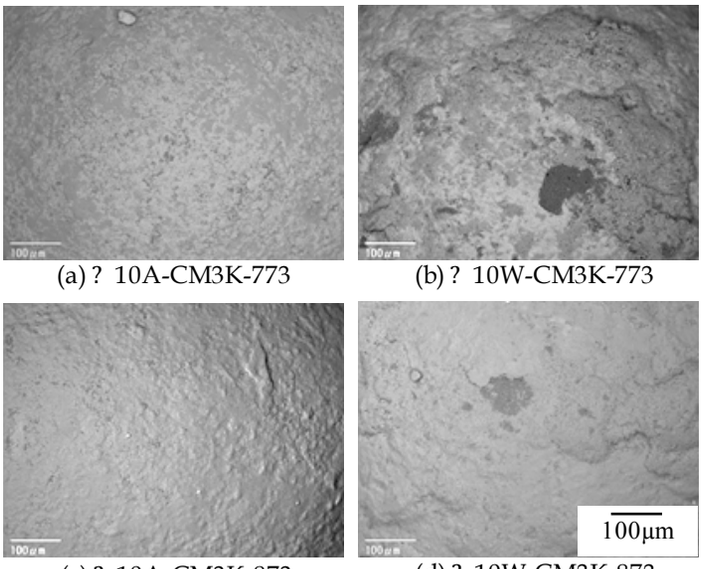

(a) ? 10A-CM3K-773 (b) ? 10W-CM3K-773

(c) ? 10A-CM3K-873 (d) ? 10W-CM3K-873

Figure 29. Surface SEM images of the samples fabricated by 2-step MCT and the following high-temperature oxidation

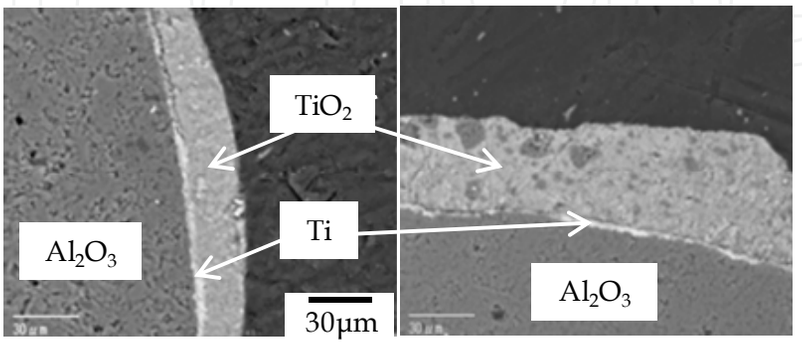

(a) ϕ 10A-CM3K-873 (b) ϕ 10W-CM3K-873

Figure 30. SEM images of the cross sections of the samples fabricated by 2-step MCT and the following high-temperature oxidation

Fig. 31 shows the XRD patterns of the samples fabricated by 2-step MCT and the following high-temperature oxidation at 673 and 873 K. For all the samples, Ti peaks and anatase TiO_2 peaks were detected while the later was rather weak due to its small loading amounts during the second step in 2-step MCT. When oxidation temperature was 873 K, the peaks of rutile TiO_2 were detected which means rutile TiO_2 was formed in the high-temperature oxidation. For the sample Φ 10W-CM6K-673 K, a weak peak of rutile TiO_2 at about 27.5º (2θ) was be found. It indicates that rutile TiO_2 formed when oxidation temperature was 673 K although the amount was rather small.

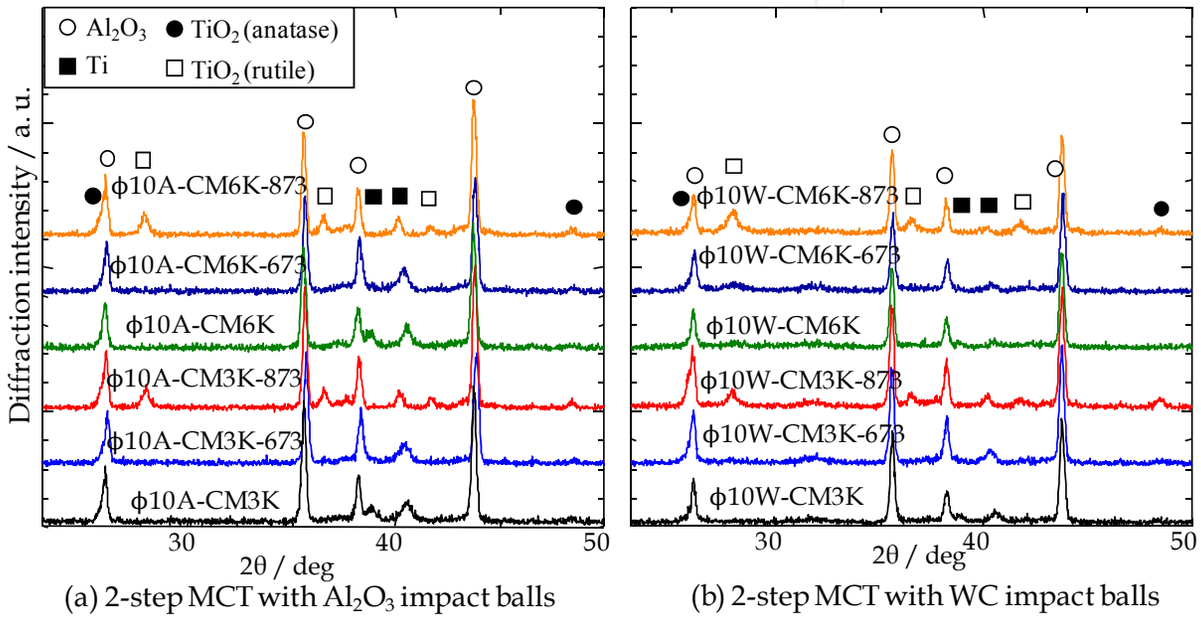

Figure 31. XRD patterns of the samples fabricated by 2-step MCT and the following high-temperature oxidation

3.3.3. Photocatalytic activity of the TiO_2/Ti composite films

The degradation rate constants, *k* as a function of oxidation temperature are shown in Fig. 32. For the samples fabricated by 2-step MCT with Al_2O_3 impact balls (Fig. 32(a)), they showed their highest photocatalytic activity when oxidation temperature was 673 K. When the 2nd MCT was 3 h, the composite films showed the greatest photocatalytic activity. On the other hand, for those fabricated by 2-step MCT with WC impact balls (Fig. 32(b)), the samples showed the similar evolution of photocatalytic activity except the Φ 10W-CM3K samples. However, their photocatalytic activity was much lower than those fabricated by 2-step MCT with Al_2O_3 impact balls. It may relate to the smaller loading amounts of anatase TiO_2 as WC impact balls exerted greater impact force and resulted in the exfoliation of the adhered TiO_2.

The improvement of photocatalytic activity should result from the microstructure and phase evolution of the composite films. As discussed in Fig. 31, Ti films were oxidized partly and rutile TiO_2 was formed when oxidation temperature was 673 K and anatase TiO_2 was reserved at that temperature. Therefore, a composite microstructure of Ti, anatase TiO_2 and rutile TiO_2 was formed. Charge separation effect and mixed crystal effect might work which can improve photocatalytic activity (Cao et al., 2009). With the increase of oxidation temperature to 873 K, the volume ratio of rutile TiO_2 in the composite films increased. It might lead that the charge separation effect and mixed crystal effect were restrained and therefore decreased the photocatalytic activity of the composite films.

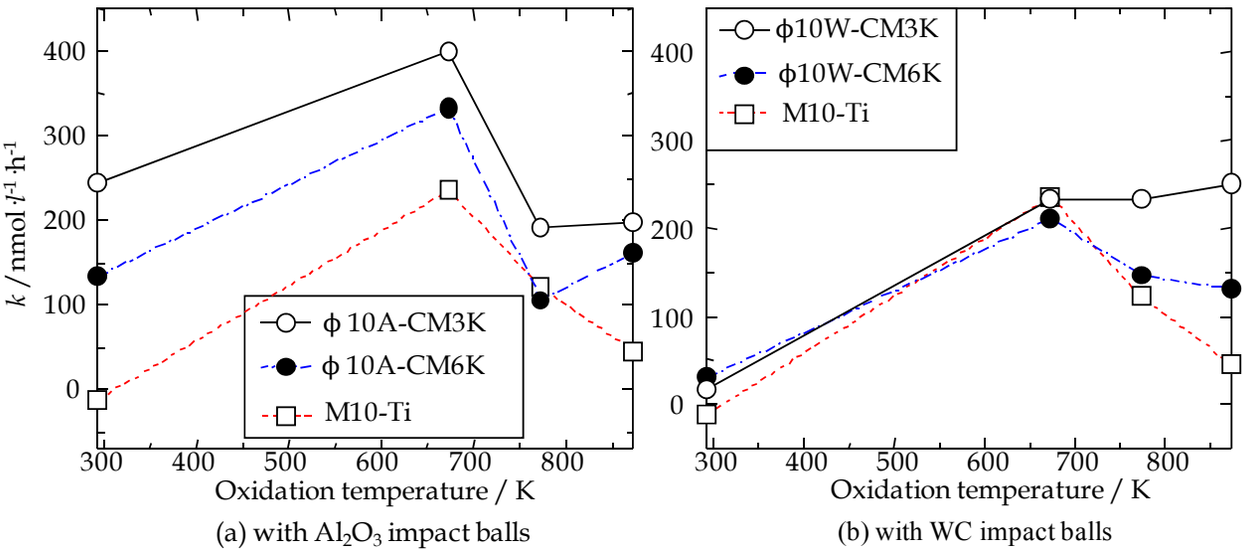

Figure 32. Degradation rate constants, *k* as a function of oxidation temperature

3.4. TiO_2/Cu composite photocatalyst films

In this section, we will describe and discuss the fabrication of TiO_2/Cu composite films by 2-step MCT. The composite films were characterized by XRD and SEM. The formation of Cu films and TiO_2/Cu composite films was also examined. The photocatalytic activity of the composite films was evaluated by measuring the degradation rate constants, *k* of MB under the UV irradiation.

3.4.1. Fabrication of TiO_2/Cu composite films

TiO_2/Cu composite films were fabricated by 2-step MCT as shown in Fig. 15. Firstly, Cu films were fabricated. The source materials and the experimental condition are listed in Table 6. To improve the production efficiency, Cu powders with different average diameters were used as the coating materials. Meanwhile, the loading amounts of Cu powder and the

rotation speed was also changed as shown in Table 6. Secondly, TiO_2/Cu composite films were fabricated. 15 g Cu film-coated Al_2O_3 balls and 13 g anatase TiO_2 powder with the average diameter of 7 nm (ST-01, Ishihara Sangyo, Japan) were used as the substrates and the coating material respectively. To make the composite films stronger, 20 Al_2O_3 impact balls with the diameter of 10 mm were simultaneously put into the bowl. The rotation speed was set at 400 rpm and the 2nd MCT time was 1, 3, 6 and 10 h.

Experiment number	Cu powder mass [g]	Cu purity [%]	Average size of Cu [μm]	Al_2O_3 ball mass [g]	Al_2O_3 ball purity [%]	Rotation speed [rpm]
1	80	99.8	40	60	93.0	400
2	40	99.8	10	60	93.0	480

Table 6. Source materials and experimental conditions for fabrication of Cu films by MCT

3.4.2. Characterization of TiO_2/Cu composite films

Fig. 33 shows the appearances of the Cu-coated Al_2O_3 balls after MCT at 400 rpm with the relevant parameters in the experiment number 1 shown in Table 6. It can be seen that the color of the samples changed from white to red brown with the increase of 1st step MCT time. It means that more Cu powder adhered to the surfaces of Al_2O_3 balls. SEM results revealed that Cu films in this experimental condition were formed when it came to 54 h. Fig. 34 shows the appearances of the samples after 2-step MCT. The color of the samples also changed with the increase of 2nd step MCT time. It indicates that the loading amounts of TiO_2 in the composite films changed. The SEM images of the cross sections of the samples are given in Fig. 35. TiO_2 adhered to Cu films (Fig. 35 (a)) and some Cu particles inlaid into TiO_2 films (Fig. 35 (b)). Therefore, it can be said that a composite microstructure of TiO_2 and Cu formed.

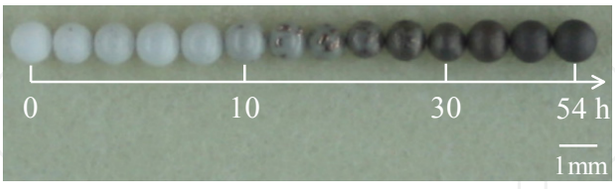

Figure 33. Appearances of the Cu-coated Al_2O_3 balls after MCT

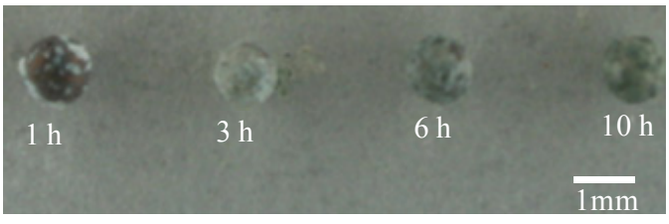

Figure 34. Appearances of the samples after 2-step MCT

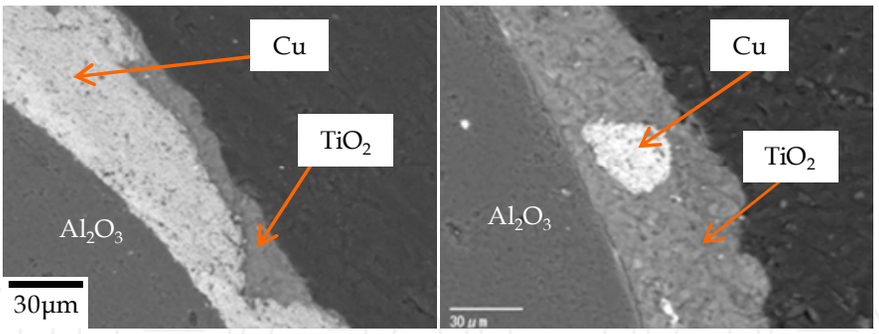

Figure 35. SEM images of the cross sections of TiO_2/Cu composite films fabricated by 2-step MCT with different the 2nd step MCT times

3.4.3. Photocatalytic activity of TiO_2/Cu composite films

MB solution concentration evolution in the evaluation of the photocatalytic activity of TiO_2/Cu composite films is shown in Fig. 36. The concentration of MB solution with the Cu film-coated Al_2O_3 balls was found to increase slightly with increase of UV irradiation time. It means Cu films did not have photocatalytic activity. On the other hand, under the action of TiO_2/Cu composite films and UV irradiation, the concentration of MB solution decreased in varying degrees. It suggests the composite films showed photocatalytic activity. For TiO_2/Cu composite films with 3 h of 2nd step MCT time, the MB solution concentration decreased to the minimum value after the same UV irradiation time for all the composite films. The degradation rate constants, k is illustrated in Fig. 37. The degradation rate constants, k increased with the increase of 2nd step MCT time and reached the peak value when it came to 3 h. After that, the degradation rate constants, k decreased with the increase of 2nd step MCT time. It means that the TiO_2/Cu composite films fabricated during MCT with 3 h of 2nd step MCT time showed the greatest photocatalytic activity for all the composite films.

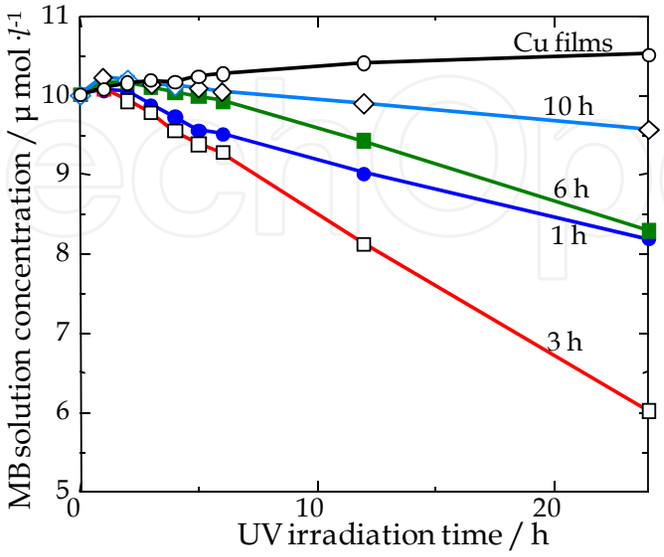

Figure 36. Evolution of MB solution concentration as a function of UV irradiation time in the evaluation of photocatalytic activity of TiO_2/Cu composite films

The photocatalytic activity of TiO_2/Cu composite films should relate to the loading amounts of TiO_2 in the composite films. With increase in 2nd step MCT time, the loading amounts of TiO_2 increased. When it came to 3 h, the loading amounts of TiO_2 might reach the peak value. After the maximum value, TiO_2 that adhered to Cu films began to peel off. The more the loading amounts of TiO_2 that deposited on Cu films, the higher the photocatalytic activity. In other words, the photocatalytic activity of TiO_2/Cu composite films should be proportional to the loading amounts of TiO_2 in the composite films. The formation of TiO_2/Cu composite microstructure is considered to be another reason why the photocatalytic activity of the composite films was improved. After formation of the interface of TiO_2/Cu, electrons in the conduction of TiO_2 will migrate to Cu films through the interface, which can decrease the recombination rate of electron-hole pairs in TiO_2. It may result in the improvement of charge separation efficiency (Rengaraj et al., 2007). Then, more electrons are trapped in Cu films for reduction reaction and more holes are held in the valence band of TiO_2 for oxidation reaction.

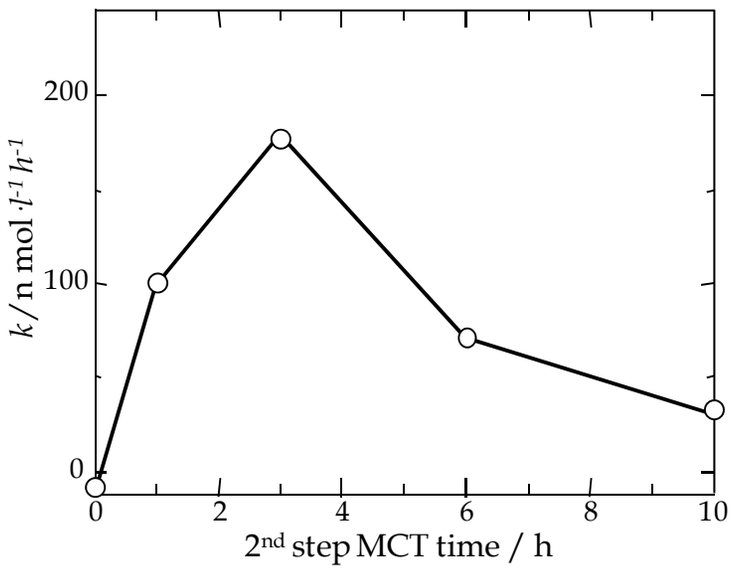

Figure 37. Degradation rate constants, *k* as a function of the 2nd step MCT time

4. Formation process of Cu films during MCT

Although Cu films and TiO_2/Cu composite films were fabricated by MCT, the formation process and its mechanism of Cu films are still unknown. Therefore, the formation process and its possible mechanism were examined and will be discussed in this section.

Because the formation process of Cu films happens in a closed and invisible bowl, it is difficult to determine the evolution of the films. However, it was considered to relate to the collision, friction and welding among the Cu powder particles, the inner wall of the bowl and the ceramic grinding mediums (Lü et al., 1995; Maurice and Courtney, 1990; Maurice and Courtney, 1994; Chattopadhyay et al., 2001). By now, we have tried to analyze the evolution of Cu films by observing the change of ceramic substrates. Fig. 38

shows the SEM images of Cu-coated Al_2O_3 balls after MCT. The areas of dark and light color correspond to alumina and copper respectively. More Cu particles adhered to the surfaces of Al_2O_3 balls with the increase of 1st step MCT time. When it came to 54 h, continuous Cu films formed and the thickness was about 10 μm. In other words, the surfaces of Al_2O_3 balls were totally coated by Cu films. The result is in good agreement with that in Fig. 33.

The coverage of Al_2O_3 ball surface with Cu is illustrated in Fig. 39. The evolution of Cu films during MCT can fall into five ranges. In the first range, the coverage hardly increased. However, Al_2O_3 balls became dark. Micron-sized Cu particles on the surfaces of Al_2O_3 balls were not found by SEM. It means that a small quantity of Cu atom clusters might transfer to the surfaces of Al_2O_3 balls. Under impact and friction force, the atom clusters adhered to the surfaces of Al_2O_3 balls and nucleated. In the second and third range, more Cu atom clusters adhered to the nuclei of Cu; these nuclei gradually grew up and could be observed by SEM (Fig. 38 (a)). Then discrete islands of Cu connected with each other (Fig. 38 (b)). The growth of Cu nuclei and the connection of discrete islands of Cu resulted in the coverage increase. After the first three ranges, the surfaces of Al_2O_3 balls were nearly coated with Cu and the coverage was close to 100%. In other words, continuous Cu films formed. Although the experiments were stopped when MCT time reached 54 h, the fourth and fifth ranges are considered to exit as the similar evolution of Fe films has been established in our published work (Hao et al., 2012). In the fourth range, the thickness of continuous Cu films may increase. As deformation of Cu particles, Cu particles become hard and adhesion between Cu particles may become difficult. Finally, exfoliation of Cu films would dominate. From the above results, the evolution of Cu films can fall into nucleation, growth of nuclei and connection, formation of continuous films and thickening, exfoliation of continuous films.

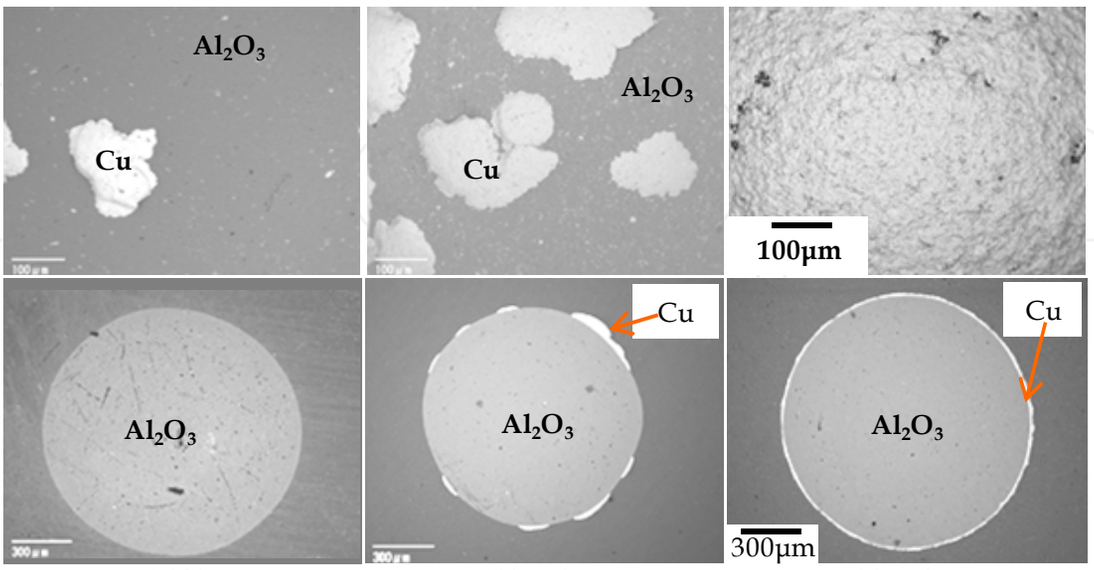

(a) 10 h (b) 22 h (c) 54 h

Figure 38. SEM images of the surfaces and the cross sections of Cu films fabricated by MCT

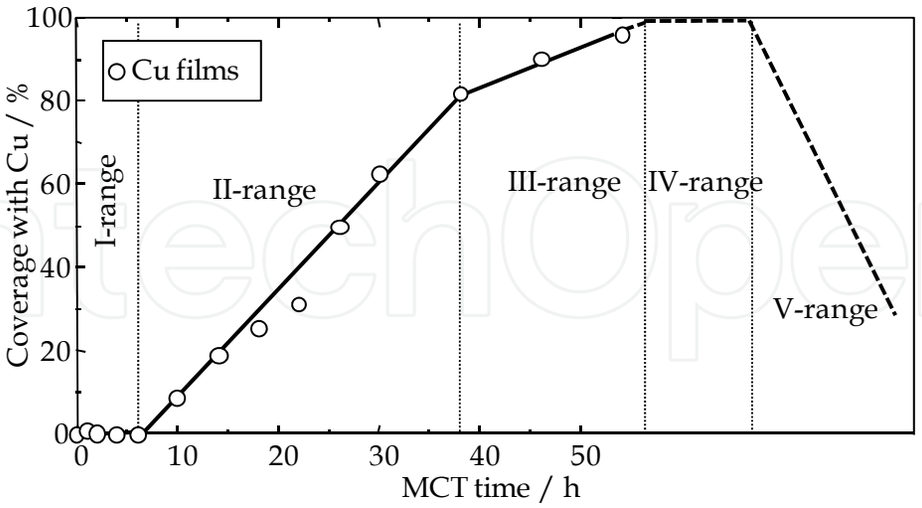

Figure 39. Coverage of Al_2O_3 ball' surface with Cu as a function of MCT time during MCT

Fig. 40 shows the SEM images of the surfaces and the cross sections of the Cu-coated Al_2O_3 balls after MCT with 480 rpm. It can be observed that continuous Cu films formed when MCT time was 20 h and the average thickness of the films was about 80 μm. Compared with the fabrication of Cu films with Cu powder of 40 μm in average particle size by MCT at 400 rpm (Fig. 38(c)), the fabrication of Cu films with Cu powder of 10 μm in average particle size by MCT at 480 rpm was quicker. In other words, the condition of Cu powder of 10 μm in average particle size and a rotation speed of 480 rpm accelerated the formation of Cu films.

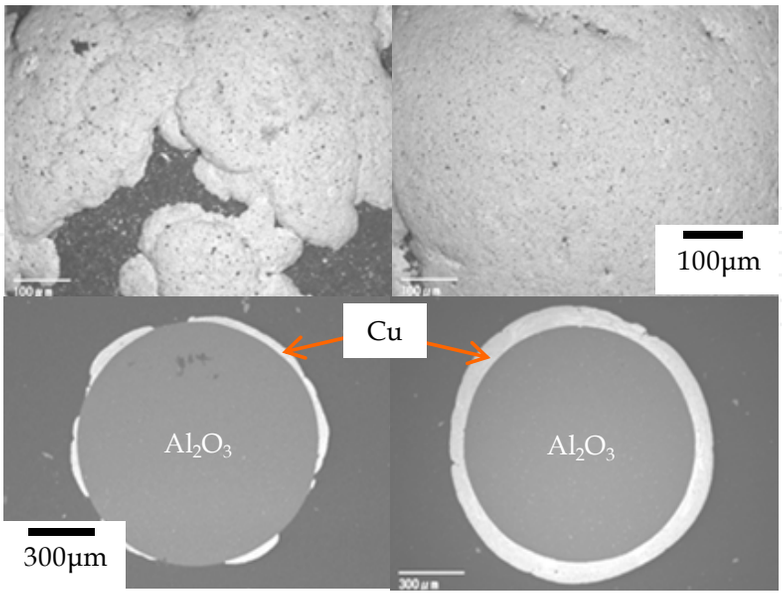

Figure 40. SEM images of the Cu-coated Al_2O_3 balls fabricated with Cu powder of 10μm in average particle size by MCT at 480 rpm

5. Prospect of MCT

Compared with the traditional film coating techniques such as PVD and CVD, our proposed mechanical coating technique (MCT) shows many advantages including inexpensive equipments, simple process, low preparation cost and large specific area, among others. In addition, it can be performed in air atmosphere at ambient temperature. It can not only fabricate metal/alloy films but also nonmetal/metal composite films such as TiO_2/Ti composite photocatalyst films. It is expected to fabricate other functional film materials in the near future.

We will continue to advance the development of MCT in the fabrication of composite films and promote their applications. Our main research subjects within next few years are listed as follows.

1. Analysis on evolution and the relevant mechanism of metal films
2. Theory construction on film formation and numerical simulation
3. Fabrication of visible light-responsive TiO_2/metal composite films
4. Improvement on photocatalytic activity of TiO_2/metal composite films
5. Application investigation of TiO_2/metal composite films in sterilization, environment purification, and so on.

Author details

Yun Lu
Graduate School & Faculty of Engineering, Chiba University, Japan

Liang Hao
Graduate School, Chiba University, Japan

Hiroyuki Yoshida
Chiba Industrial Technology Research Institute, Japan

6. References

Cao, Y. Q.; Long, H. J.; Chen, Y. M.; Cao, Y. A. (2009). Photocatalytic activity of TiO_2 films with rutile/anatase mixed crystal structures. Acta Physico-Chimica Sinica, Vol. 25,pp. 1088-1092.

Chattopadhyay, P. P.; Manna, I.; Talapatra, S.; Pabi, S. K. (2001). A mathematical analysis of milling mechanics in a planetary ball mill. Materials Chemistry and Physics, Vol. 68, pp. 85-94.

Farahbakhsh, I.; Zakeri, A.; Manikandan, P.; Hokamoto, K. (2011). Evaluation of nanostructured coating layers formed on Ni balls during mechanical alloying of Cu powder. Applied Surface Science, Vol. 257, pp. 2830-2837.

Gupta, G.; Mondal, K.; Balasubramaniam, R. (2009). In situ nanocrystalline Fe-Si coating by mechanical alloying. Journal of Alloys and Compounds, Vol. 482, pp. 118-122.

Hao, L.; Lu, Y.; Asanuma, H.; Guo, J. (2012). The influence of the processing parameters on the formation of iron thin films on alumina balls by mechanical coating technique. Journal of Materials Processing Technology, Vol. 212, pp. 1169-1176.

Japan Industrial Standard, JIS K 7194, 1994.

Japan Industrial Standard, JIS R 1703-2, 2007.

Kobayashi, K. (1995). Formation of coating film on milling balls for mechanical alloying. Materials Transactions, Vol. 36, pp. 134-137.

Lu, Y.; Hirohashi, M.; Zhang, S. (2005). Fabrication of oxide film by mechanical coating technique, *Proceedings of International Conference on Surfaces, Coatings and Nanostructured Materials*, Aveiro, Portugal.

Lu, Y.; Yoshida, H.; Nakayama, H.; Hao, L.; Hirohashi, M. (2011 a). Formation of TiO_2/Ti composite photocatalyst film by 2-step mechanical coating technique. Materials Science Forum, Vol. 675-677, pp. 1229-1232.

Lu, Y.; Yoshida, H.; Toh, K.; Hao, L.; Hirohashi, M. (2011 b). Performance improvement of TiO_2/Ti composite photocatalyst film by heat oxidation treatment. Materials Science Forum, Vol. 675-677, pp. 1233-1236.

Lu, Y.; Hao, L.; Toh, K.; Yoshida, H. (2012). Fabrication of TiO_2/Cu composite photocatalyst thin film by 2-step mechanical coating technique and its photocatalytic activity. Advanced Materials Research, Vol. 415-417, pp. 1942-1948.

Lü, L.; Lai, M. O.; Zhang, S. (1995). Modeling of the mechanical-alloying process. Journal of Materials Processing Technology, Vol. 52, pp. 539-546.

Mattox, D. M. (2010). Handbook of physical vapor deposition (PVD) processing, William Andrew Publication, ISBN 978-0-8155-2037-5, Burlington, USA

Maurice, D. R.; Courtney, T.H. (1990). Physics of mechanical alloying, a first report. Metallurgical and Materials Transactions, Vol. A21, pp. 289-303.

Maurice, D. R.; Courtney, T.H. (1994). Modeling of mechanical alloying: part I. deformation, coalescence, and fragmentation mechanisms. Metallurgical and Materials Transactions, Vol. A25, pp. 147-158.

Pierson, H. O. (1999). Handbook of chemical vapor deposition, Noyes Publications and William Andrew Publication, ISBN 0-8155-1432-8, New York, USA

Rengaraj, S.; Venkataraj, S.; Yeon, J. W.; Kim, Y.; Li, X. Z.; Pang, G. K. H. (2007). Preparation, characterization and application of Nd-TiO2 photocatalyst for the reduction of Cr (VI) under UV light illumination. Applied Catalysis, Vol. B 77, pp. 157-165.

Romankov, S.; Sha, W.; Kaloshkin, S. D.; Kaevitser, K. (2006). Formation of Ti-Al coatings by mechanical alloying method. Surface Coatings Technology, Vol. 201, pp. 3235-3245.

Suryanarayana, C. (2001). Mechanical alloying and milling. Progress of Materials Science, Vol. 46, pp. 1-184.

Yoshida, H.; Lu, Y.; Nakayama, H.; Sano, H.; Hirohashi, M. (2008). Fabrication and evaluation of composite photocatalytic film by mechanical coating technique, *Proceedings of the 6th International Forum on Advanced Material Science and Technology*, Hong Kong, China

Yoshida, H.; Lu, Y.; Nakayama, H.; Hirohashi, M. (2009 a). Analysis of Ti films fabricated by mechanical coating technique (In Japanese). Journal of Materials Science Society of Japan, Vol. 46, pp. 141-146.

Yoshida, H.; Lu, Y.; Nakayama, H.; Hirohashi, M. (2009 b). Fabrication of TiO_2 film by mechanical coating technique and its photocatalytic activity. Journal of Alloys and Compounds, Vol. 475, pp. 383-386.

Yoshida, S.; Taga, Y.; Kinbara, A.; et al. (2008). Handbook of thin films, Ohmsha Publication, ISBN 978-4-274-20519-4, Tokyo, Japan